THE STUDY OF THE SWELLING PROPERTY OF BITUMINOUS COAL

by

Wei Fun Sung

Submitted in Partial Fulfillment

of the Requirements for the Degree of

Bachelor of Science

at the

MASSACHUSETTS INSTITUTE OF TECHNOLOGY

May, 1977

Signature of Author _____
Department of Chemical Engineering

Certified by _____
J. B. Howard, Thesis Supervisor

Accepted by _____
J. E. Vivian
Departmental Committee on
Undergraduate Theses

ACKNOWLEDGEMENTS

I would like to thank my thesis supervisor, Professor Jack Howard, for his advice and his patience in granting me extra time to complete this paper.

Other people whose help and encouragement I deeply appreciate include Ted Bush, for his assistance in collecting samples, and other friends, for their part in the typing effort.

The Study of the Swelling Property of Bituminous Coal

1. SUMMARY

The purpose of this study was to determine the swelling property of of Pittsburgh No. 8 seam coal under different experimental conditions. The experimental variables were the average initial particle size of coal particles and the peak temperature of the laminar flow reactor employed to obtain particulate samples for this study.

The study has shown that the average swelling ratio of the particulate sample increases with the average initial particle size. A least square method was used to correlate the linear relationship between the average swelling ratio and the average initial particle size for unagglomerated particulate samples formed at a constant peak temperature, and the correlation was satisfactory.

The study has also shown that there is a close relationship between the rate of thermal decomposition of coal and the swelling ratio of the particulate samples, namely, they both peak at a certain temperature. Attempts were made to correlate the average swelling ratio of the samples with the average temperature of the laminar flow reactor at a constant average initial particle size. The correlation was not very good, probably due to a lack of information on the reactor average temperature corresponding to the average maximum swelling of the particulate samples, as well as a lack of data obtained at the low temperature of the laminar flow reactor.

2. INTRODUCTION

2.1 General Background

Recently, there has been a growing commercial interest in the use of coal and coal derived fuels. During the past years, intensive research has been directed toward the development of improved coal utilization procedures, in particular processes for converting coal to clean gases and liquids, i.e. gasification and liquefaction. The main task of the coal utilization development is to investigate processes for upgrading the hydrogen to carbon ratio of the material. The typical atomic hydrogen to carbon ratio of coals is 0.6 to 1.0 whereas, for example, it is 4.0 for natural gas and about 1.8 or 1.9 for crude oil. The task of upgrading can be accomplished to a certain extent by coal pyrolysis.

In coal pyrolysis, which is thermal decomposition accomplished by elevating the temperature, the coal is converted to a hydrogen rich volatile fraction and a carbon rich solid residue. The residue will then react with hydrogen gas rapidly during or just after volatile release (Anthony and Howard, 1976). There have been many models developed to describe the rate of thermal decomposition and volatile yields of coals upon heating, and the most satisfactory model developed is Anthony's Multiple Reaction Model.

2.2 Objective And Motivation

Coal can be characterized as plastic or nonplastic depending upon whether it goes through a plastic region upon thermal heating within

the experimental operating conditions of interest, namely, rapid heating rates of 10^3 °C/sec to 10^4 °C/sec, pressure ranges of 1 atm to 69 atm and temperature ranges of 400° C to 1000° C. It has been observed that some coals swell under moderate and rapid heating, and the swelling phenomenon is associated with plastic coals. Some workers have observed swelling amount to as much as a 4000 per cent increase in volume (Sinnatt, 1928 1929). The swelling of coal particles will be a potential problem in the scaling up of environmentally and economically sound pyrolysis processes, especially those based on the use of fluidized beds.

Fluidized beds consists of two phases, a bubble phase and a particulate phase. The properties of fluidized bed are strongly dependent on the particle size, i.e. the superficial incipient fluidization velocity, the pressure drop across the bed, and the proportion of gas passing upward via the bubble phase and the particulate phase. In the case of plastic coals, particles will swell and become sticky as they rise, and both the swelling and agglomeration of sticky particles will change the behavior of the bed. Therefore, it is desirable to study the swelling property of the plastic coal under different experimental conditions.

The primary objectives of this study can be stated as follows:

1. To experimentally determine the effect of initial coal particle size on the swelling ratio (final diameter/initial diameter) under a specific set of experimental conditions, namely, inert atmosphere, constant peak temperature, constant reaction time and constant heating rate.

2. To experimentally determine the effect of temperature on the

swelling ratio under the following conditions, namely, inert atmosphere, constant reaction time, and constant initial particle size.

A laminar flow reactor of the Badzioch type was used to obtain particulate samples for the present study of swelling ratio. The reasons for the choice were: The dispersion of coal particles in a gaseous medium of a flow reactor is similar to that of a fluidized bed, but a laminar flow reactor has exceedingly better control of reaction time, and the agglomeration of fresh feed can be minimized with good techniques of feeding. Since the temperature of the laminar flow reactor is not constant, the average and the peak reactor temperature were used to evaluate data obtained in this study. The heating rate was in the range of 43200° C/sec to 64000° C/sec depending upon the peak temperature used. (See Appendix A-5).

The major experimental variables of the study were the sizes of coal particles and the peak or the average temperature of the reactor. Nine different particle size distributions of Pittsburgh No. 8 seam coal were examined which had the following initial average particle sizes (affective diameter in μm) : 267, 202, 164, 145, 122, 89, 71, 46 and 41. Five different peak temperatures were employed: 960°, 830°, 750°, 650° and 600°C. The reaction atmosphere was helium at a pressure of 1 atm. The reaction time was approximately 1/3 second.

3. BACKGROUND MATERIAL

During the past years, efforts have been made to study the physical behavior of plastic coal at an elevated temperature with a rapid heating

rate. The commonly observed sequence of events is: fusion, intumescence, and solidification. More specifically, upon heating a bed of crushed plastic coal, the coal particles first soften and fuse. As thermal decomposition becomes appreciable, the bed swells and becomes foam-like (Brown and Waters, 1966; Chermin and Van Krevelen, 1957; Gibson and Gregory, 1971; Waters, 1962). Under rapid heating conditions, a bed of particles resembles a boiling liquid (Anthony, 1974). The intumescence is generally believed to be the formation of gas bubbles inside the coal mass. After a significant part of coal has decomposed, the mass solidifies into coke and it has a much higher melting point than the original coal (Audibert, 1927). Here the main concern is the physical behavior of bituminous coal particles upon heating, i.e. swelling property, under different experimental variables. Hence, it is of interest to review some of the studies on the physical properties of plastic coals which have contributed to the present understanding of swelling of bituminous coal upon heating.

3.1 Coal Plasticity

The chemical complexity of coals is partly due to heterogeneous petrographic components of the organic part. Neavel (1975) has made a study on the effect of marcerals on coal plasticity, and he concluded that the plasticity of bituminous coal is primarily attributed to the presence of marcerals exinite and vitrinite.

Early work done by Audibert (1927) has shown that the plastic state is transient, and the rate of heating greatly affects the point of initial

fusion or plastic state. He has concluded that the initial melting point is always higher for higher heating rates, and is independent of coal rank.

The rate of heating also has a significant impact on the maximum fluidity and duration of the plastic region. Van Krevelen's study (1956) has concluded that the broadening of duration of plastic region and the increase of maximum fluidity are associated with the increasing heating rate. When heated at a constant rate of 0.05°C/sec, the plastic region lies between 420°C and 500°C. Figure 3-1a illustrates the effect of heating on coal fluidity for heating rates from 0.7°C/min to 7.2°C/min.. In the same literature, Van Krevelen (1956) has also determined that the development and decaying of fluidity and the rate of thermal decomposition upon heating both depend on heating rates. (See Figure 3-1b). Walters (1962) has also performed a similar study on the relationship between rates of thermal decomposition and the development and decaying of fluidity. Figure 3-2 demonstrates the typical behavior of fluidity and rate of thermal decomposition at a heating rate of 3°C/min, and it strongly indicates that the rate of thermal decompositon controls the fluidity of plastic coals.

3.2 Rheological Property of Coal

Since temperature is an experimental variable, the viscosity-time-temperature relationship in pyrolysis should be studied.

In Water's investigation (1962) of rheological properties of a number of plastic coals, he observed that plastic coals behave like a

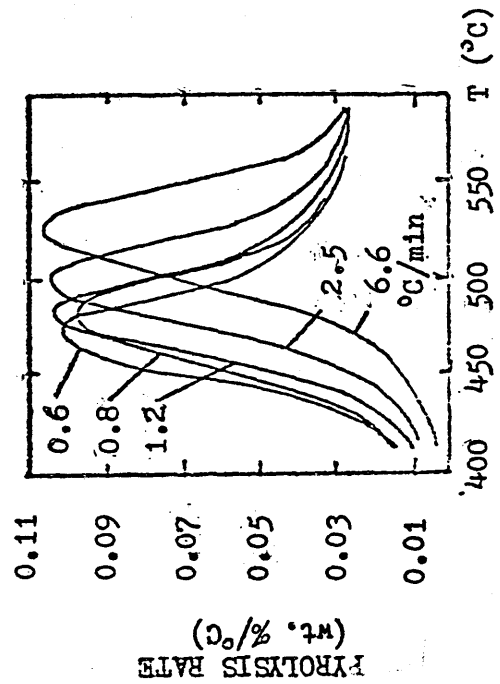

Figure 3-1b Pyrolysis rate as a function of heating rate (Van Krevelen, 1956)

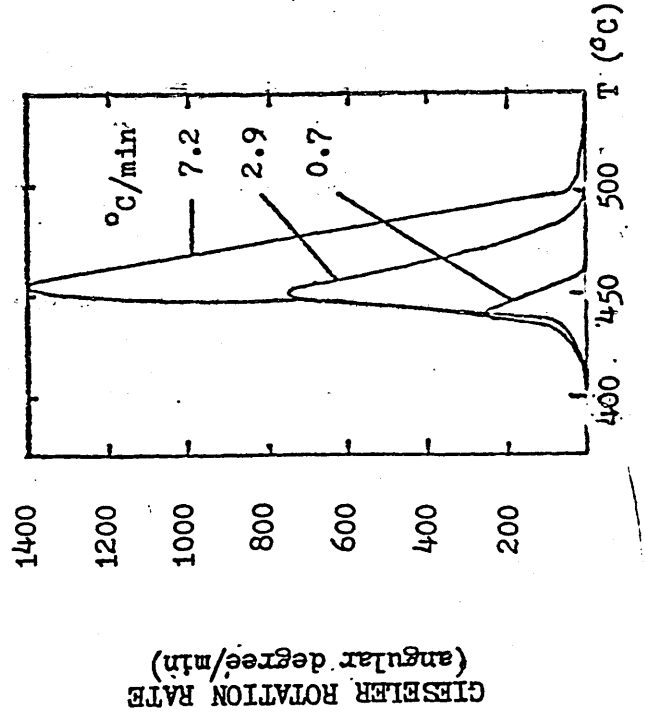

Figure 3-1a Fluidity as a function of heating rate (Van Krevelen, 1956)

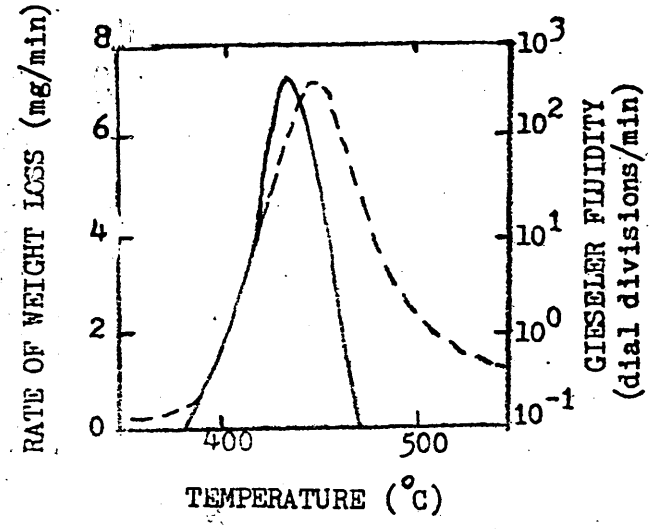

Figure 3-2 Fluidity (full line) and decomposition (broken line) curves (heating rate, 3°C/min) (Waters, 1962)

Newtonian fluid under normal stress during the early stage of fusion. Based on this observation, he applied the Andrade equation for the liquid viscosities

$$\eta = A \exp(E/RT) \quad \text{(Andrade, 1930)},$$

and found that the plastic region of the early stage of fusion obeys the relationship well. The activation energies of flow for coals, E's, were determined experimentally, and were found to be in the range of 50 - 100 kcal/mole. The values are high for ordinary Newtonian fluids (Waters, 1962).

The Andrade equation is applicable only to plastic regions where the thermal decomposition is negligible because the chemical changes of coal in that region are not significant. At the plastic region where the thermal decomposition is active, there is a drastic change in the chemical composition of coal particles; hence the Andrade equation will no longer be valid.

Recognizing the deficiency of the equation, Lewellen (1975) postulated the following PRM viscosity temperature relationship.

$$\eta = \eta_1 (d\alpha/dt)^{-1}$$

where $d\alpha/dt$ is rate of pyrolysis, and η_1 is an empirically determined parameter. The value of η_1 used in his study was 3×10^6 sec/pse. The close relationship between the fluidity and the rate of thermal decomposition physically justifies the above relationship.

3.3 Physical Structure of Char Particles

A rigorous X-ray study of the internal structure of a wide range of coals was made by Hirsch (1954). Hirsch has developed a model

to characterize the structure of coals. According to his model, bituminous is classified as having a " liquid structure " which is characterized by the near absence of pores. But, an examination of char products of thermal decomposition revealed high large-scale porosity within the char particles (Woods et al., 1967; Feldmann et al., 1971). The striking difference can be explained by the formation and motion of bubbles inside the coal particle during pyrolysis. Under a hot stage microscope, the particles may be seen to soften, become round, and swell while large bubbles of gas repeatedly break through the particle surface as pyrolysis continues (Ergun et al., 1959; Woods et al., 1967; Spackman and Berry, 1968). Large-scale porosity is presumably formed by entrapped gas bubbles (Woods et al., 1967; Feldmann et al., 1971).

The development of cenospheres, which occurs when plastic coals are heated at moderate or rapid rates in the absence of air, represents the extreme case of large scale porosity (Newall and Sinnatt, 1924, 1926, 1927; Sinnatt et al., 1927; Sinnatt, 1928, 1929; Mason and Schora, 1967; Lightman and Street, 1968; Street et al., 1969). The cenosphere is essentially a hollow and swollen char particle (see Figure 5-3a), with a reticulated structure containing two major parts, ribs and windows. The ribs are brownish-black substances and the windows are transparent brownish thin films. A more detailed examination of cenospheres in the windows revealed the presence of minute forms. (See Figure 3-3).

In the Newall and Sinnatt study (1924), it was observed that the formation of cenoshperes under a moderate heating rate in the absence

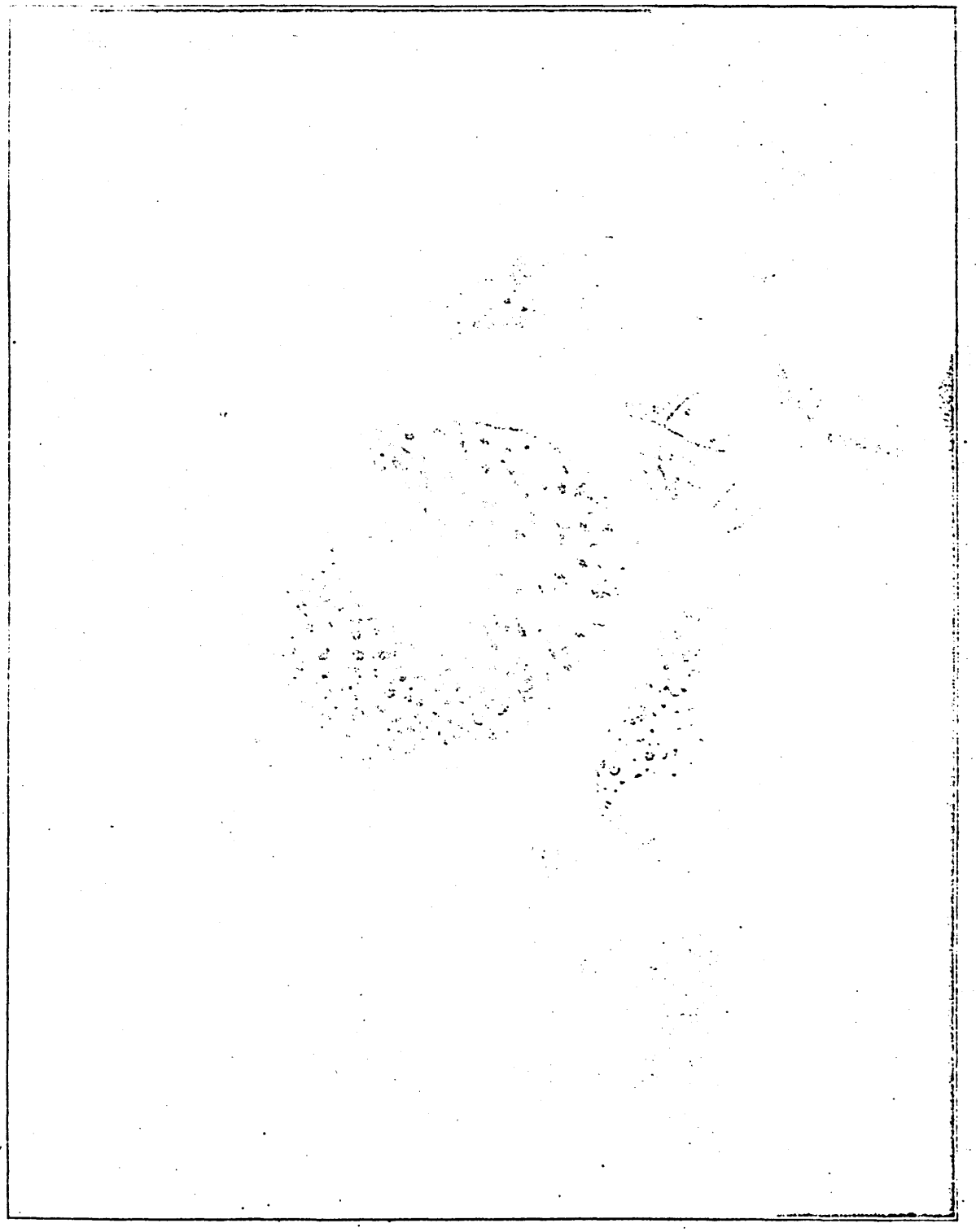

Figure 3-3 Cenosphere formed at 650 C (360X)
(Newall and Sinnatt, 1924)

Showing minute forms

of air is temperature dependent. The ribbed window structure could not be clearly detected until 570°C to 600°C was reached. With an increase in temperature, the detection of cenoshperes is easier and the network structure increases in size. The increase in size of the network structure causes the rib and window structures to become thinner. The windows become nearly colorless at high temperature. However, when the coal particles were heated to 800° or 900°C, the distinct ribbed window structure could not be detected; the particles become opaque and shrank in size.

In another study of effects of different atmospheres upon the structure of cenospheres by Sinnatt, McCulloch and Newall (1927), it was observed that cenospheres formed in the presence of hydrogen were essentially structurally identical with those formed in the presence of nitrogen. When an atmosphere of steam was used, the formation of ribs and windows was partially inhibited.

In general, the porosity of the fine structure of char increases with an increase in temperature. But, the accessibility of these pores to the penetrant molecules does not follow the same trend. In plastic coals, the accessibility of pores to the penetrant molecules displays a sharp minimum in the plastic region of the coal (600°C-1000°C) because of an absence of continous pores, and increases below 500°C to 600°C. (Franklin, 1949a, 1949b; Bond and Spencer, 1958; Van Krevelen, 1961; Evans, 1970).

3.4 Multiple Reaction Model

There are many kinetic models developed to describe the temperature

dependent behavior of coal pyrolysis. The Multiple Reaction Model developed by Anthony (1974) has been proven to be in good agreement with the experimental data. The first assumption of the model is that the overall rate of volatile yield is the sum of a large number of parallel first order reactions:

$$\frac{dV}{dt} = \sum_{i}^{\infty} \frac{dV_i}{dt}$$

$$\frac{dV_i}{dt} = k_i(V_i^* - V_i), \text{ where } k_i = k_i^o \exp(-E_i/RT).$$

In the above expression, subscript i denotes a particular reaction and no subscript denotes overall reactions. V is the total weight fraction of volatiles evolved at time t, and V^* is the total weight fraction of V at infinite time. V_i and V_i^* are similarly defined for each reacting species. E_i and k_i^o are the activation energy and the preexpontential factor respectively in the above rate constant of Arrhenius type. k_i^o is to be determined experimentally.

The second assumption of the model is that a Gaussian Distribution with mean activation energy of E_o and standard deviation σ is used to determine the activation energy distribution of each reaction.

$$f(E) = \left[\sigma(2\pi)^{1/2}\right]^{-1} \exp\left[-(E-E_o)^2/2\sigma^2\right]$$

Combining the two assumptions, and assuming k_i is identical for all reactions, Anthony showed that

$$\frac{V^* - V}{V^*} = \int_o^{\infty} \exp\left[\int^t -k\,dt\right] f(E)dE$$

The experimentally determined values of E_o, σ, k_i^o and V^* have been found

to be 54.8 kcal/mole, 17.2 kcal/mole, 1.67 x 10^{13}/sec and 0.462, respectively, for Pittsburgh No. 8 bituminous seam coal (Anthony and Howard, 1976).

Althought Anthony's model successfully described the temperature dependent behavior of bituminous coal pyrolysis, there is a decreasing trend of volatile yield with an increase in particle size. (See Figure 3-4). Suuberg (1977) also observed a similar trend of volatile yields with particle sizes in his study using the captive heating technique to obtain the volatile yields. To explain the apparent deviation of volatile yields from the Multiple Reaction Model at large particle sizes, a secondary reaction mechanism has been postulated, namely, reaction between volatile generated by coal decomposition with the remaining char particle to form solids and gases during the volatile escape. The solid formed by the secondary reaction is deposited inside the remaining particle, thereby decreasing the total weight loss of the volatile (Anthony, et al., 1974). With increased particle size, the volatile must travel farther before escaping and thus has more time to react with the char particle. Consequently the extent of secondary reaction is increased and the volatile yield is reduced. Lewellen (1975) assumed that the rate of secondary reaction is a first order reaction and is proportional to the pressure of volatile inside the coal particle.

$$\text{rate of secondary reaction: } q_d = k_d P$$

where k_d is the reaction rate constant of Arrhenius type.

3.5 Mode of Transport of Volatile

The macroscopic evidence of the formation and motion of bubbles inside

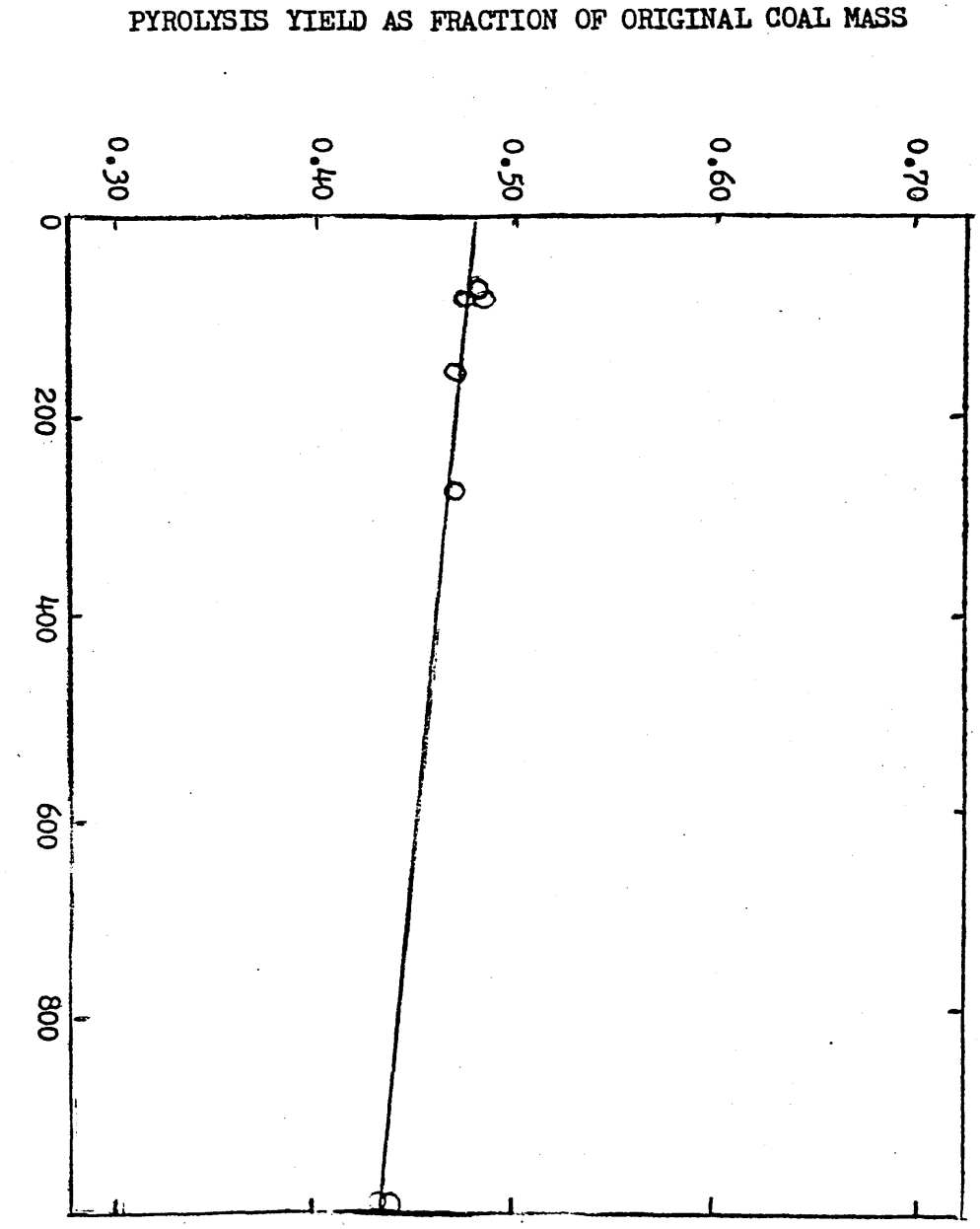

Figure 3-4 Effect of particle size on product yields from bituminous coal. (Anthony, 1974)

the plastic coal particle leads to the assumption that bubble transport is an important mode of transport of volatile from plastic coals during coal pyrolysis. An analytical model has been developed by Lewellen (1975) to describe the behavior of bubbles inside the plastic coal. He pictured the sequence of bubbles inside the coal particle as: (1) initiation of bubbles, (2) growth of bubbles and (3) bubble death.

3.51 Bubble Initiation

Two mechanisms of bubble initiation inside the plastic coal have been proposed. One is analogous to initiation of bubbles from a vapor filled cavity at the liquid-solid interface (Lewellen, 1975), the second is analogous to bubble initiation in boiling water (Attar, 1977). Lewellen's study of bubble initiation used the first mechanism. Instead of developing an exact analytical solution to describe the behavior of bubble initiation, he adopted a probability distribution function for bubble generation in the coal particle. He assumed that the function depends on four variables: volumetric rate of bubble generation ($d\alpha/dt$) particle viscosity (η), the distance to the nearest surface to which volatiles could otherwise escape (d_{min}), and the initial radius of the bubble (a_o).

Lewellen's Probability Distribution Function of Bubble Generation:

$$\Lambda_b(r,\theta,\phi) = \text{Min}\left\{ (k_b/\eta)(\lambda_{a_o})(d\alpha/dt)(d_{min})(\Delta V)(\Delta t)(\Delta a_o),\ 1 \right\}$$

Figure 2-5 shows the concepts of bubble generation. λ_{a_o} is the initial bubble size probability distribution function, and k_b is an empirical bubble generation constant. (See Figure 3-5 for concepts of bubble generation).

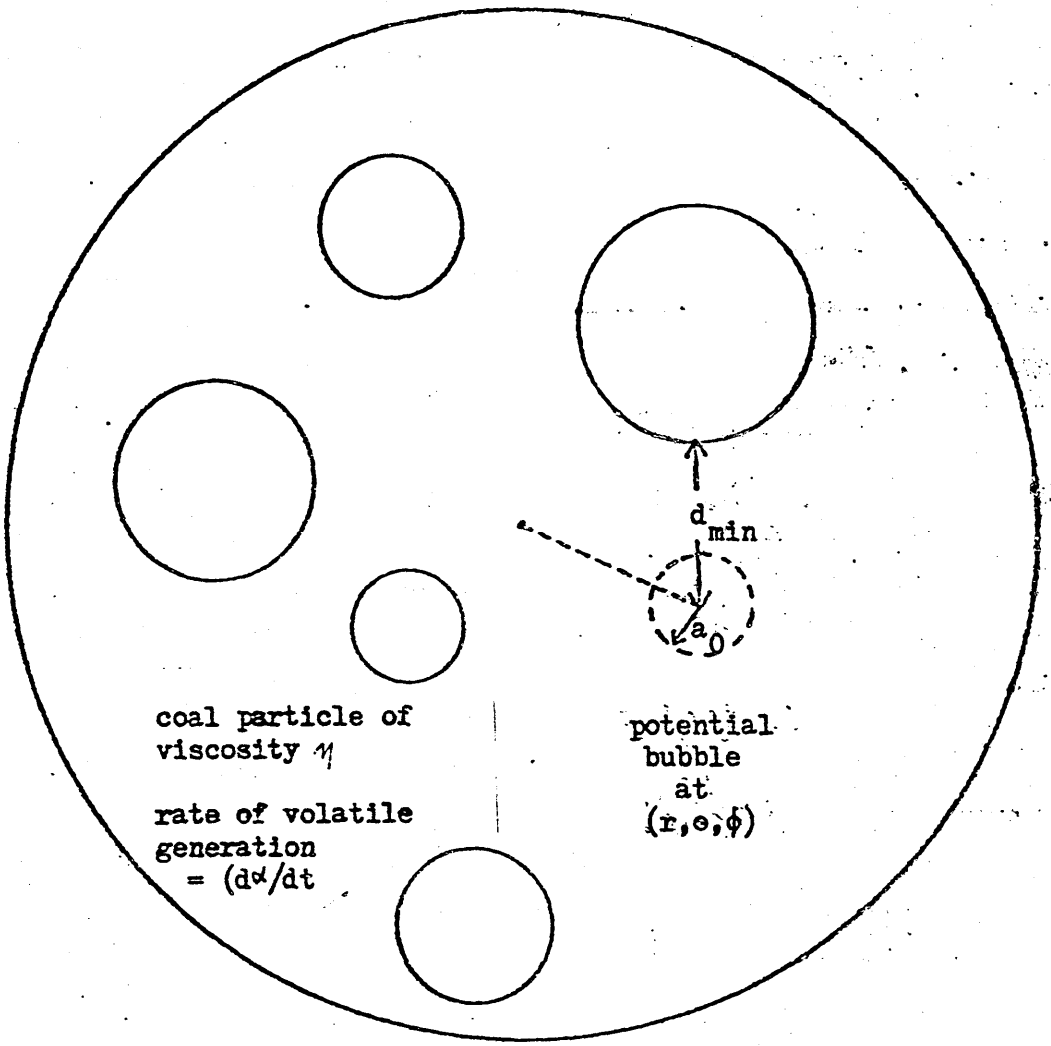

Figure 3-5 Concepts of bubble generation (Lewellen, 1975)

3.52 Bubble Transport

Lewellen's lengthy development of bubble growth (1975) assumes the following physical conditions of a plastic coal particle.

1. The coal particle is homogeneous, isotropic and spherical.
2. The coal particle is isothermal for all time.
3. The particle is subject to no external forces other than pressure.
4. The coal particle has two homogeneous constituents, a volatile phase and a particle phase.

Based on the above assumptions and other assumptions, i.e. ideal behavior of volatile, negligence of the density of volatile phase compared to that of the particle phase, incompressibility of both volatile and particle phase, and constant surface tension for the inner and outer shell of bubble surface, an analysis of momemtum transport was performed to determine the rate of bubble growth, $\dot{a}$. (See Equation 3-2 on Table 3-1). In addition to the hydrodynamic consideration of the bubble growth, Lewellen (1975) also developed a model to describe the rate of increase of mass of volatile inside the coal particle due to instantaneous transport of newly generated volatile to the bubbles, which in turn will increase the rate of bubble growth. In his study, the mass flux of volatile transport is assumed to be equally distributed on the total surface area available, this is, the surface areas of bubbles plus the surface area of the coal particle. Equation 3-3 show the mass flux per unit area, F. Lewellen (1975) has also considered the effect of secondary reaction of the rate of mass accumulation inside the bubble.

He assumed that only solids formed from secondary reactions. By a simple mass balance, the net mass flux to a bubble is determined. (See Equation of 3-4 on Table 3-1). Equation 3-13 on Table 3-1 shows the expression of the secondary reaction rate constant. Equation 3-12 describes the total rate of the secondary reaction per particle. The concepts of bubble growth and concepts of secondary reaction chemistry are shown on Figure 3-6 and Figure 3-7.

3.53 Bubble Death

Two mechanisms of bubble death have been proposed by Lewellen (1975), namely, death through escape and death through intersection. (See Figure 3-8 for concepts of bubble death). For death through escape, an instantaneous expulsion of bubble contents from the coal particle is assumed when the bubble wall reaches a critical distance (δ_p) from the surface of the particle and the volume of the particle is instantaneously contracted by an amount equal to the bubble volume. This is only true for coal particles that are in their plastic region and have high fluidity. In death through intersection, the walls of two bubbles touch each other and the two bubbles combine into one. The location of the newly formed bubble will depend on the locations of the bubbles before they intersect and the volumes of the individual bubbles. (See Equation 3-7, 8, 9, 10 on Table 3-1). The size of the newly formed bubble will be determined from the equilibrium condition; that is, the rate of the bubble growth is zero. (See Equation 3-11 on Table 3-1).

The total volume of the coal particle at any time is the sum of the volume of the particle phase plus the total volume of the bubble phase or

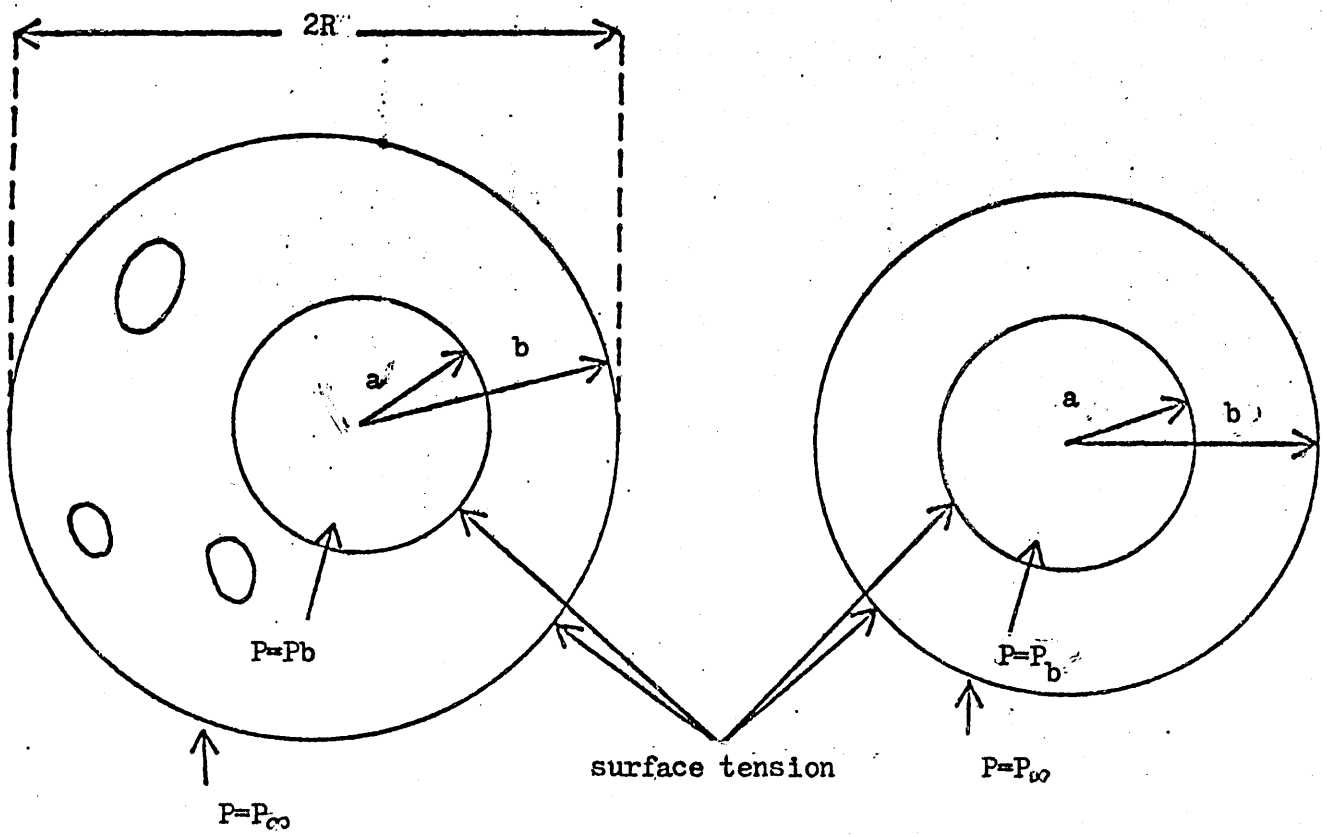

(a) the physical situation (b) the modeled situation

Figure 3-6 Concepts of bubble growth
(Lewellen, 1975)

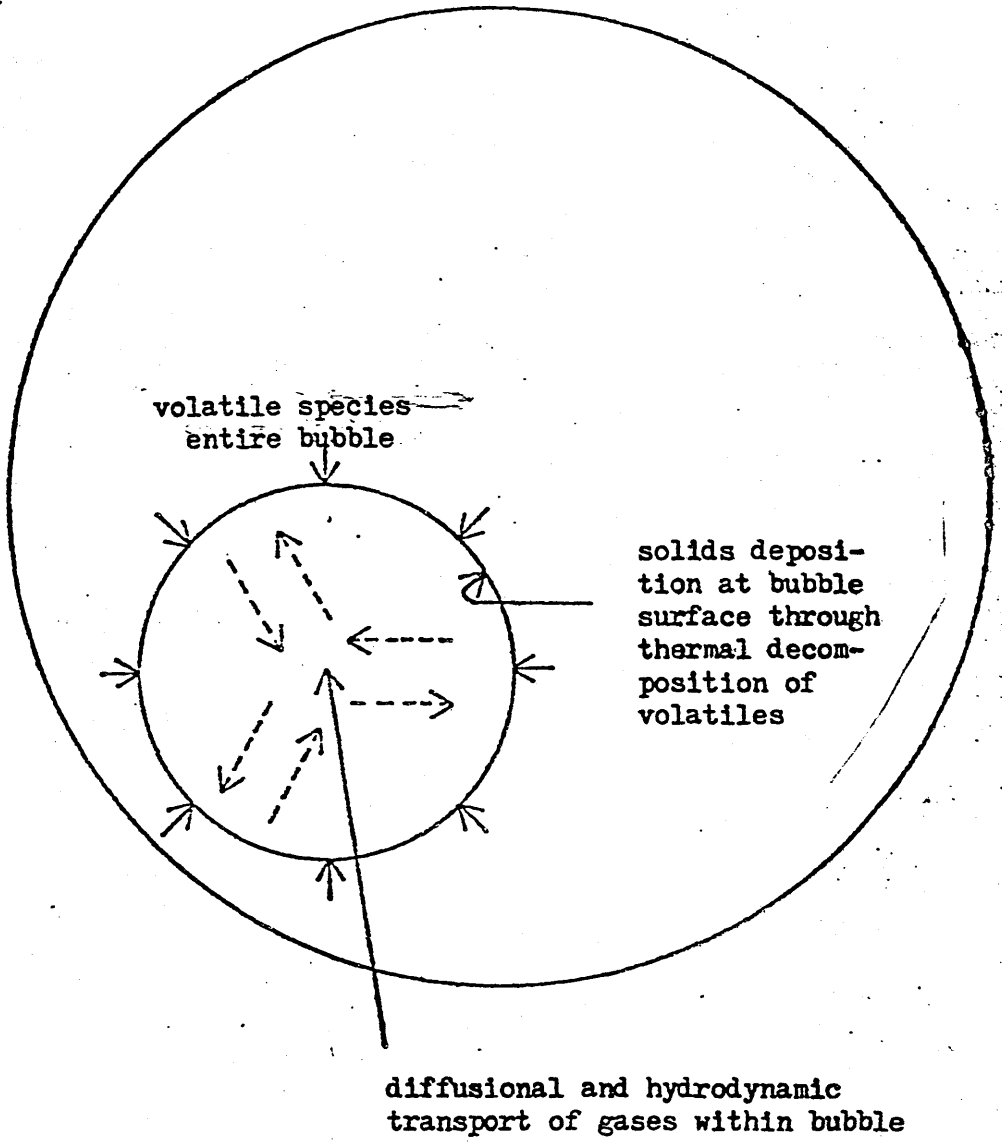

Figure 3-7 Concepts of secondary reaction chemistry. (Lewellen, 1975)

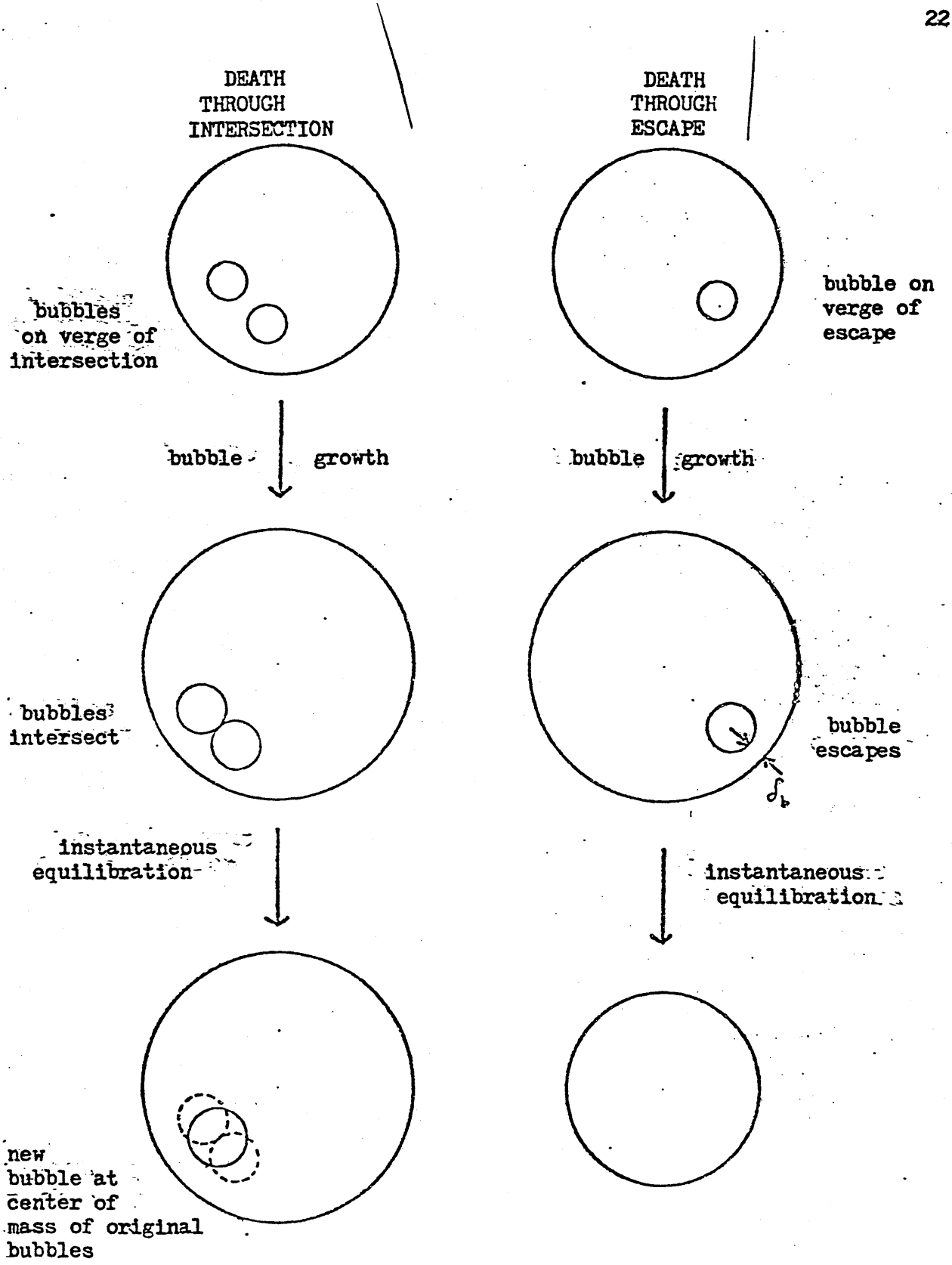

Figure 3-8 Concepts of bubble death (Lewellen, 1975)

Table 3-1

Summary of Lewellen's Modelling Equations
(Lewellen, 1975)
(See Appendix A-8 for nomenclature)

APPLICATION	EQUATION NUMBER	EQUATION
BUBBLE INITIATION	3-1	$\Lambda_b = \text{Min}\{ (k_b/\eta)(\lambda_{ao})(d\alpha/dt)(d_{min})\Delta V \Delta t \, \Delta a_o, \, 1 \}$
BUBBLE GROWTH individual bubble momentum balance	3-2	$\dot{a}_i = \dfrac{(3\nu_i RT)/(4\pi a_i^2 W) - 2\sigma(1 + a_i/b_i) - a_i/b_i) - a_i P_\infty}{4\eta \left(1 - (a_i/b_i)^3\right)}$
mass flux definition	3-3	$F = M_o(d\alpha/dt)/(4\pi R^2 + 4\pi \sum_i a_i^2)$
individual babble mass balance	3-4	$\dot{\nu}_i = 4\pi a_i^2 (F - q_d)$
OVERALL PARTICLE DYNAMICS surface weight loss mass balance	3-5	$M_p = 4\pi R^2 F$
particle volume calculation	3-6	$V_p = \sum_i (4\pi/3)\, a_i^3 + (1/\rho_p)(M_p - W - \sum \nu_i)$
BUBBLE DEATH		
	3-7	$\nu_j = \nu_i + \nu_j$
	3-8	$x_j = (x_i \nu_i + x_k \nu_k)/\nu_j$
death through intersection	3-9	$y_j = (y_i \nu_i + y_k \nu_k)/\nu_j$
	3-10	$z_j = (z_j \nu_j + z_k \nu_k)/\nu_j$
	3-11	$0 = (3\nu_j RT)/(4\pi a_j^2 W) - 2\sigma(1 + a_j/b_j) - a_j P_\infty$
death through escape	None	
SECONDARY REACTION KINETICS	3-12	$Q_d = (3RT\, k_d \nu_i)/(w \cdot a_i) = 4\pi a_i^2 q_d$
	3-13	$k_d = k_d^o \exp(-E_d/RT)$

the volatile phase. The size of the coal particle is calculated from the total volume assuming the coal particle is a sphere.

3.6 Particle Size Trend Prediction And Temperature Trend Prediction

In Lewellen's simulation (1975) of bubble transport inside the coal particle, he incorporated Anthony's Multiple Reaction Model for the estimation of the rate of volatile generation of one coal particle, and PRM viscosity prediction with the equations listed on Table 3-1 to predict the trend of swelling ratio of coal particles and the extent of secondary reaction as particle size increases. The conditions of his simulation were: initial particle temperature of 298° C, final particle temperature of 1000° C, heating rate of 10000° C/sec, pressure of 10 atm, initial bubble size of 5×10^{-6} cm, $\eta_1 = 3 \times 10^{-6}$ sec/psc and $k_b = 6 \times 10^{10}$ cm^{-2}. The results of his simulation are presented in Figure 3-9. It is clearly shown that the swelling ratio increases with particle size, and the volatile yield decreases with particle size. The increasing trend of the swelling ratio is nearly linear in the particle size range of 120 μm to 230 μm, and it then increases monotonically above the particle size range of 230 μm. The linearly increasing trend is primarily due to an increase in the fraction of the number of generated bubbles trapped in the particle as a result of a longer distance each particle has to travel before escaping. As the particle size increases beyond 230 μm, the effect of the secondary reaction becomes more significant, and a greater loss of bubble mass results. In turn the bubble volume is reduced because of the smaller rate of bubble growth. Therefore, instead of a linear increase, the trend shows a non-linear but a monotonic increase in swelling ratio as the particle size increases above 230 μm.

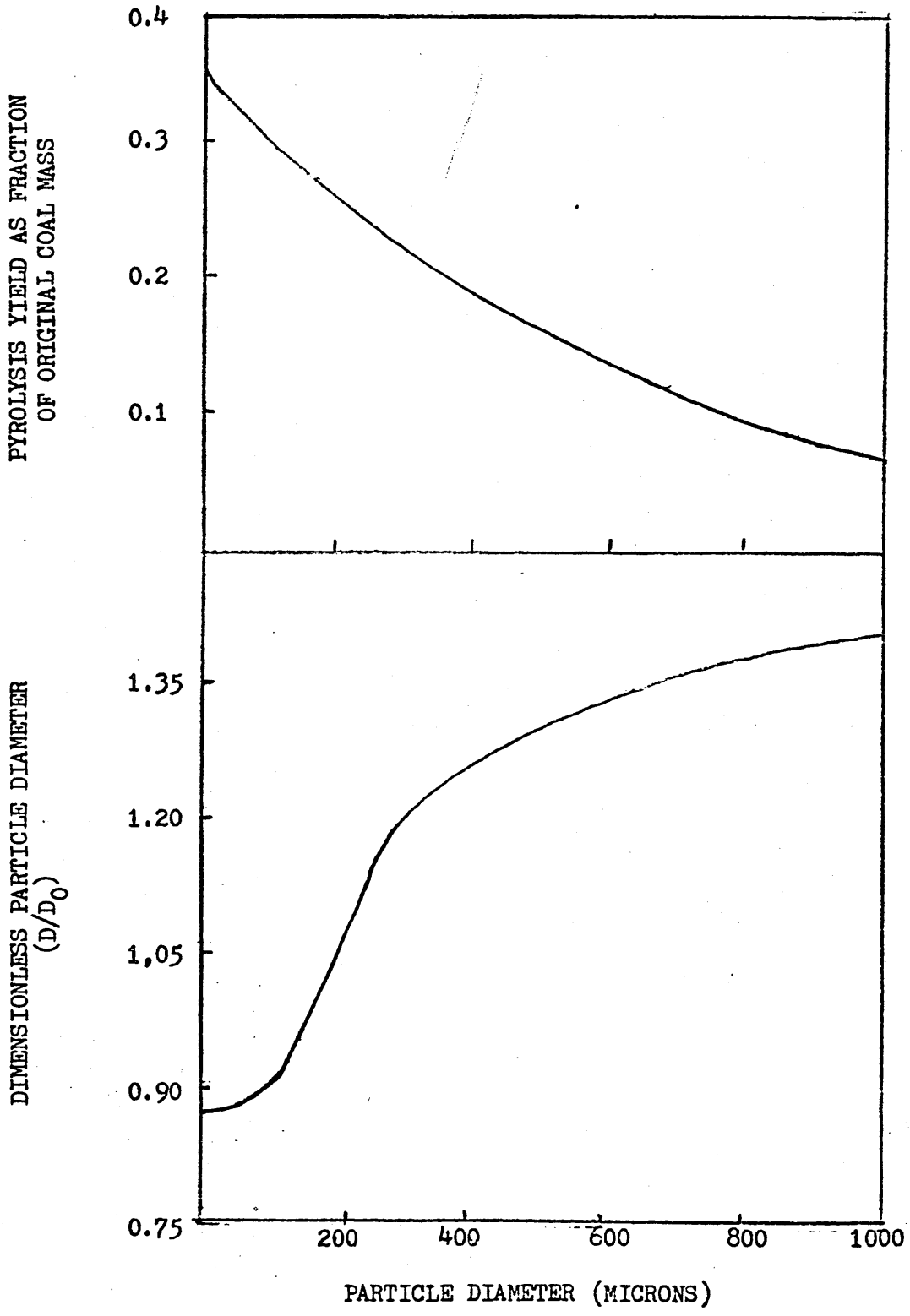

Figure 3-9 Predicted trends in volatile yield and particle swelling with particle size using PRM viscosity calculation. (Lewellen, 1975)

The author is not aware of any analytical solution developed to predict the effect of temperature on swelling ratio. Therefore, the effect on temperature on the swelling ratio of bituminous coal has to be determined experimentally. However, since it is believed that the rate of bubble generation inside the coal particle is partially dependent upon the viscosity and the rate of thermal decomposition of the coal particle, it was speculated that the swelling-temperature relationship would be similar to the fluidity-time-temperature or the thermal decomposition rate-time-temperature relationship in pyrolysis (see Section 3-1), namely, all of them peak at a certain temperature.

4. EXPERIMENTAL APPARATUS AND PROCEDURE

4.1 Apparatus

The laminar flow reactor needed for this study had already been constructed for used in previous research. A Microstar Light Microscope and a Transmission Electron Microscope 200 (TEM 200) were used to photograph the representative sample particles, and a TZG 3 was used for the counting of particle sizes.

4.11 Laminar Flow Reactor

A simplified diagram of the reactor employed in this study is shown in Figure 4-1. A small stream of helium carrier gas (5 - 10 cc/min) carried the sample particles through a water-cooled feed tube, 1/16 inches i.d., into the reaction tube. A vibrator was placed midway between the top of the feed tube and the top of the reaction tube to avoid plugging of the feed tube. The main gas (helium) was fed into the reaction tube

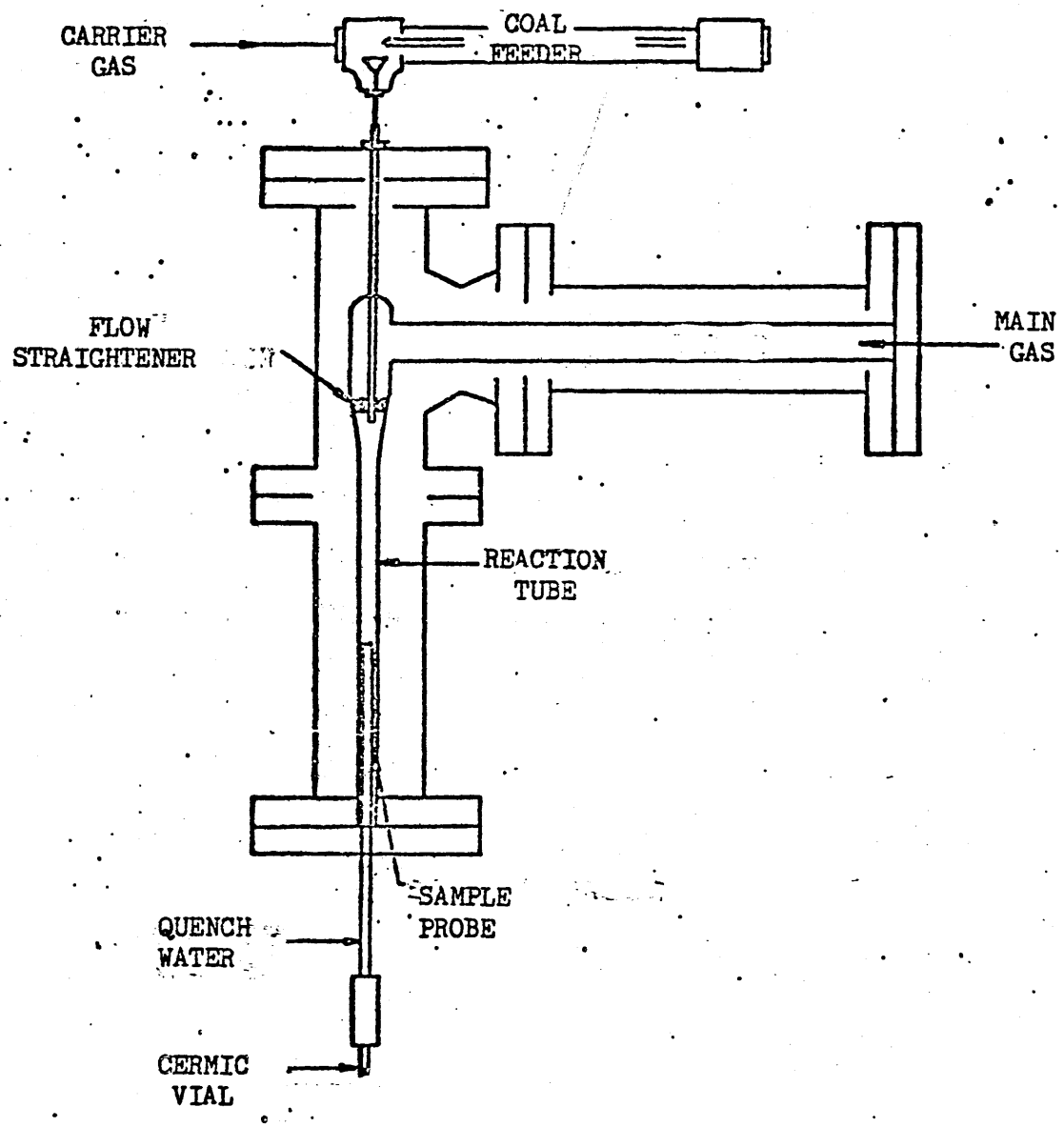

Figure 4-1 Laminar flow reactor

through an expansion chamber to insure uniformity in the gas flow. There was also a flow straightener placed at the end of the feed tube to prevent a spiral flow in the reaction tube. The flow rate of the main gas was set to insure a laminar flow in the reactor tube at the temperature of interest. (See Appendix A-3). The one inch i.d., 22 in. long reaction tube was constructed of 99.8% aluminum. The temperature profile of the reaction tube was not vertically uniform (See Appendix A-1). The lower part of the reaction tube overlapped with the sample probe, and the sample probe was water-cooled to quench the reaction; therefore, the reaction zone was only eight inches long. The temperature profile of the 8 inch long reaction zone with the insertion of the water-cooled sample probe showed no appreciable deviation from that of the 8 inch reaction zone without the insertion of the water-cooled sample probe. (See Appendix A-2). A ceramic vial was connected to the sample probe to collect the char samples for size determination.

4.12 Microstar Light Microscope & TEM 200

See the manuals of the Microstar Light Microscope and the TEM 200 for a description of the apparatus and methods of operation.

4.13 TZG 3

The TZG 3 was used to determine the average particle size of the samples of interest. The TZG 3 employed in this study is shown in Fig. 4-2 Two measuring relationships between the iris diameter and the counter number were incorporated in the TZG 3, namely, the linear and exponential

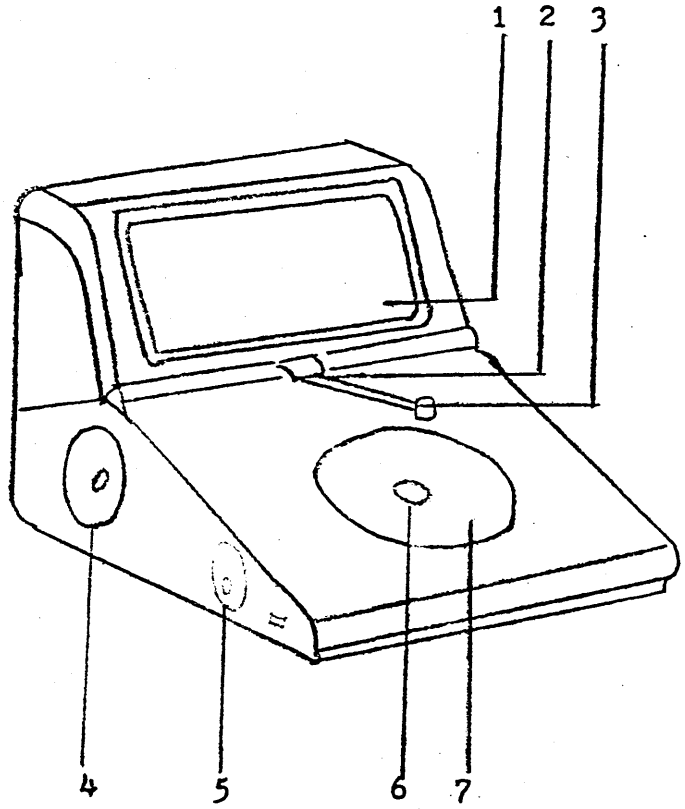

1. COUNTER NUMBER
2. KNURLED KNOB
3. PUNCHER
4. ROTARY SWITCH
5. SOCKET PLATE
6. IRIS
7. GLASS INSERT

Figure 4-2 TZG 3

relationship between the iris diameter and the counter number. The linear mode of operation is used for narrow particle size distributions, and the exponential mode of operation is used for wide particle size distributions. For each measuring mode, there are two measuring ranges, the standard range (1.2 mm to 27.7 mm) and the reduced range (0.4 mm to 9.2 mm). The TZG 3 also has two modes of recording the relationship between the counter number and the iris diameter, namely,the distribution curve and the cumulative curve. There are eight modes of operation altogether. In this study, only two modes of operation were used: a standard linear mode of operation and a reduced linear mode of operation, both using the distribution curve.

The method of operating of the TZG 3 is very simple. After the mode of operation is chosen, the diameter of the iris is adjusted manually with the rotary switch to cover the area of the particle image of interest until the two areas coincide. To record the size of the particle image on the counter number, the foot switch is pressed. This makes a mark on the image and releases the number.

4.2 Procedure

4.21 Preparation of Closely Size-Graded Coal Particles

In order to examine the swelling property of different particle sizes of Pittsburgh Seam Coal, closely size-graded coal particles are needed. The molecular sieve method was employed to narrow the particle size distributions. (See Appendix A-4 for the relationship between

U.S. Standard mesh # and particle size). Nine different closely size-graded coal samples were obtained and each sample was transferred to a crucible and stored separately in a small dessicator partially filled with silica gel to prevent contamination from air moisture.

4.22 Preparation of Char Sample

After the proper size range had been chosen, approximately 20 mg of the coal sample was spread carefully on the center portion of the feed belt of the reactor. The length of the spread was usually 3-4 inches long, and the width of the spread was approximately 1/8 to 1/16 of an inch. The exact amount of the coal charged to the reactor was determined by the weight difference between the initial and final weight of the crucible. The feed tube was closed during the process of feeding to prevent particles from entering the reaction tube prior to the start of the reaction run. After the charging of the reactor, the top of the laminar flow reactor was sealed, and a ceramic vial was connected to the sample probe. Then the flow velocity of the main gas was set at 2 ft/sec. The top of the reactor was pressurized slightly above one atmosphere with the feed tube closed to prevent back flow of the main gas in the reaction tube. The final steps were turning on the vibrator, opening up the feed tube, and turning on the feed belt. The velocity of the feed belt was set at 1 in./min. Each run lasted about 6 minutes. At the end of each run, the ceramic vial was disconnected from the sample probe and weighed before transferring the char sample to a glass bottle for storage. The weight of sample collected was calculated from the weight difference

between the initial and final weight of the ceramic vial.

4.23 Preparation of Particle Images for Size Analysis.

After the sample had been collected, a portion of it was spread uniformly on a microscope slide, and examined under the light microscope. (The procedure for char products produced at the peak temperature of 650° C was slightly different from the above. See Section 6.2.). The magnification used was 4X or 10X, depending upon the particle sizes. The representative sample sites were photographed using Type 52 Polaroid film. The number of particles photographed was about 200-300 for most of the samples. Since the swelling ratio was the main interest, the original average particle size was needed to complete the analysis. The original particle samples were photographed in a similar manner, except for the particle size distributions of 44μm - 53μm and 53 μm - 63 μm. It was felt that the average particle size of these two size distributions could not be accurately determined using the light microscope. So the TEM 200 was used to prepare particle images for the size analysis.

Before the sample could be examined under the TEM 200, it had to be placed on a grid of mesh #200. The grid was coated with a very thin film of collodion. While the coating was drying, the sample of interest was suspended in the distilled water. After the coating had been dried, a drop of the liquid-solid suspension was placed on top of the coated grid. The water was allowed to evaporate before the sample was placed inside the TEM 200 to be photographed. Finally, the plates were developed and the pictures were printed. The plate magnification used here

was 2600.

It was soon discovered that the particle size distributions of 44 μm - 53 μm and 53 μm - 63 μm had a large fraction of particle sizes much smaller than the 44 μm or 53 μm. Although all other particle size distributions had particle sizes much smaller than the lower limit of the mesh # used (probably due to adhesion of smaller particles to the larger particles), they could be ignored since the weight fraction of them was expected to be negligible compared to the rest of the particle size distribution. The problem became more pronounced as the particles decreased in size. At 44 μm - 53 μm and 53 μm - 63 μm, it was a serious problem. It was decided to ignore particle sizes smaller than 30 μm for the present study. Approximately 30 particles were used for particle size analysis in these size distributions.

4.24 Determination of Average Particle Sizes of Samples.

The 4X and 10X magnification used for the light microscope does not mean that the particle images photographed were 4X or 10X their original sizes. Therefore, the calibration of TZG 3 was needed to determine the particle sizes of the images. The method of calibration was as follows: first, a very accurate reference system was photographed for each magnification , then, the iris diameter of the TZG 3 was matched with one particular length of the magnified scale for each mode of operation of interest, and finally, the length of the iris diameter was recorded. The magnification factor was then calculated by taking the ratio of the length of iris diameter recorded to the corresponding reference length.

Each counter number of TZG 3 was then calibrated by dividing the corresponding iris diameter by the same magnification factor. (See Appendix A-7). This procedure was performed four times for different magnification and modes of operation of TZG 3. For the case of TEM 200, there was no need to calibrate the TZG 3. The magnification factor was simply the product of the magnification of particle images on the plate and the magnification of the enlarger.

After all the particle images of a char sample were recorded by TZG 3, the arithmetic averages of swelling ratio were calculated for each sample.

4.25 Determination of Fresh Feed Agglomeration.

At an early stage, it was realized that the fresh feed agglomeration of coal particles might account for the large increase in volume of char products of small particles. Most of the fresh agglomeration could not be detected under the microscope because agglomerated particles fused to form one particle. In order to determine the extent of agglomeration of coal particles, the following experiment was performed.

Approximately 0.3 mg of particles with average diameter of 41 μm were carefully spread uniformly on a microscope slide. The amount of coal particles on the slide was determined by the difference between the initial and final weight of the slide. The representative sample sites were then photographed, and the number of particles of diameter approximately equal to 30 μm or greater were counted. Then the

average number of particles per unit area of spread was calculated by dividing the total number of particles counted by the area of the photographed sites. The total number of particles on the slide was determined by multiplying the average number of particles per unit area of spread by the estimated total area of spread. The total number of particles per unit mass of the sample was calculated by dividing the total number of particles on the slide by the weight of the particles on the slide. Similarly, the experiment was carried out for the char particles with initial diameter of 41 μm at a peak temperature of 650° C. It was found that the agglomeration was more than 200 particles by assuming the weight loss was negligible in the char product. The same analysis was performed for the char particles of average initial particle sizes of 46 μm and 71 μm formed at a peak temperature of 650° C; it was found that the agglomeration was approximately 60 and 5 respectively. Since the main interest of the study was the determination of the swelling ratio of unagglomerated particles, data obtained for initial average particle size of 41 μm, 46 μm, and 71 μm were discarded from the analysis. But, there was also some question as to whether the char products obtained from the initial average particle size of 89 μm were agglomerated since some char products appeared to be agglomerations of two or more particles. (See Figures 5-5a,b,c.). Because of the uncertainty, data obtained for char particles with initial average particle sizes of 89 μm at peak temperatures of 650° C, 830° C, and 960° C were discarded.

5. RESULTS AND PHOTOGRAPHS

Table 5-1

Average Swelling Ratio of Char Particles

Peak temp. (°C)	600	650	750	830	960
Avg. temp.	550	600	700	780	900
Init. avg. part. size	Final avg. particle size/Init. avg. part. size				
D_o (μm)	D/D_o	D/D_o	D/D_o	D/D_o	D/D_o
267	1.286	1.289	1.060	1.011	0.909
202	1.080	1.568	1.045	0.954	0.821
164	1.075	1.176	0.896	0.965	--
145	--	1.083	--	--	0.865
122	0.997	1.109	0.848	0.906	--
89	0.982	1.150*	0.869	1.465*	1.158*
71	--	1.817*	--	2.180*	1.903*
46	--	4.920*	--	2.816*	2.410*
41	4.058*	6.41*	3.789*	4.24*	3.774*

-- No data collected.

* Agglomerated char products.

Table 5-2

Results of the Least Square Method for The Relationship between Swelling Ratio and Particle Size

Peak temperature °C (Average temperature)	Derived correlation
600 (550)	$D/D_o = 1.548 \times 10^{-3} D_o + 0.819$
650 (600)	$D/D_o = 1.330 \times 10^{-3} D_o + 0.832$
750 (700)	$D/D_o = 1.305 \times 10^{-3} D_o + 0.723$
830 (780)	$D/D_o = 6.158 \times 10^{-4} D_o + 0.842$
960 (900)	$D/D_o = 3.878 \times 10^{-4} D_o + 0.786$

Table 5-3

Results of the Least Square Method for The Relationship between Swelling Ratio and Average Temperature

Initial average particle size D_o (μm)	$S = (D/D_o) \times 10^2$ $A = (1/T) \times 10^4$
267	$S = 11.607\ A - 109.685$
202	$S = 13.886\ A - 137.696$
164	$S = 11.14\ A - 115.364$
122	$S = 11.355\ A - 123.613$

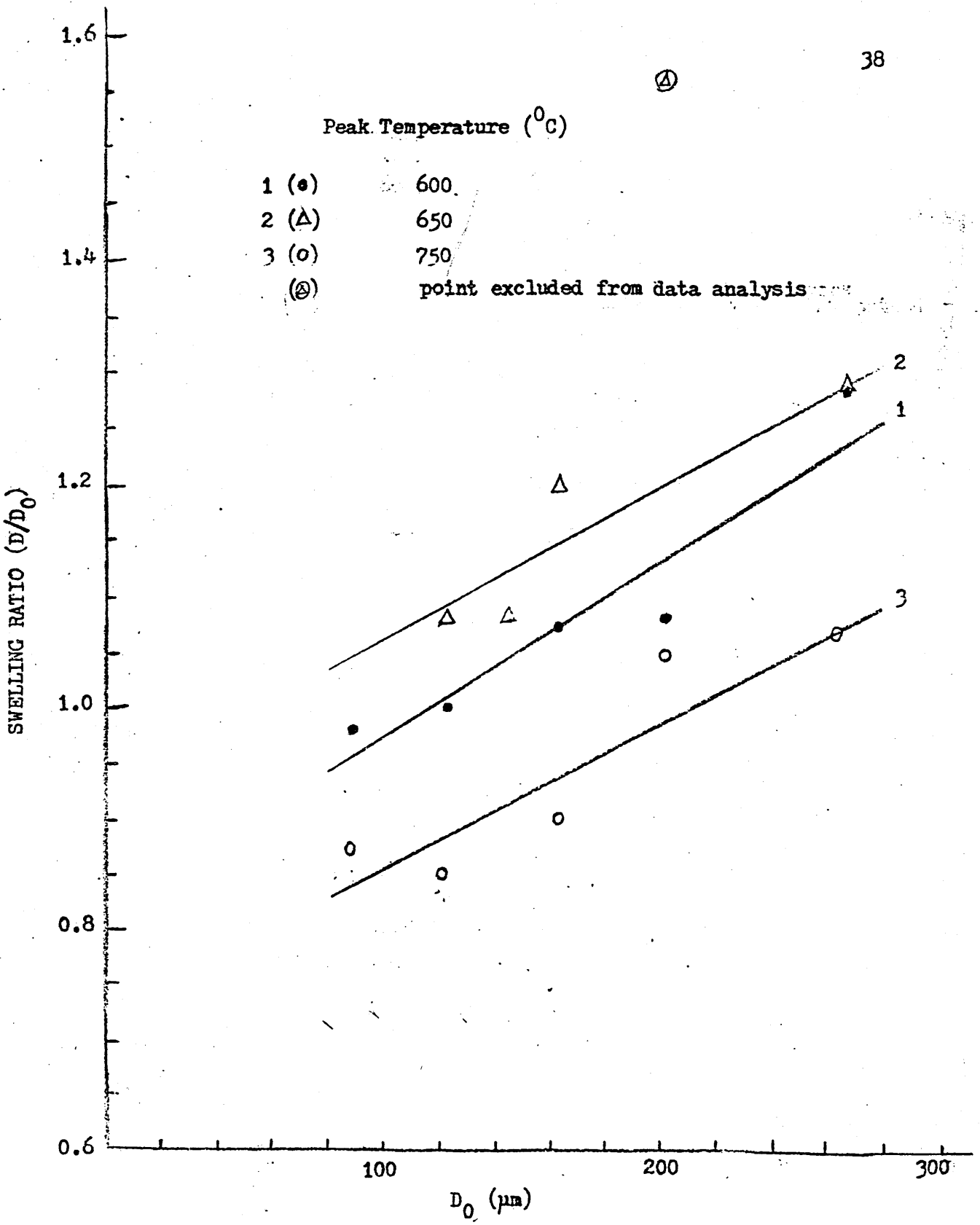

Figure 5-1a Relationship between swelling ratio and particle size

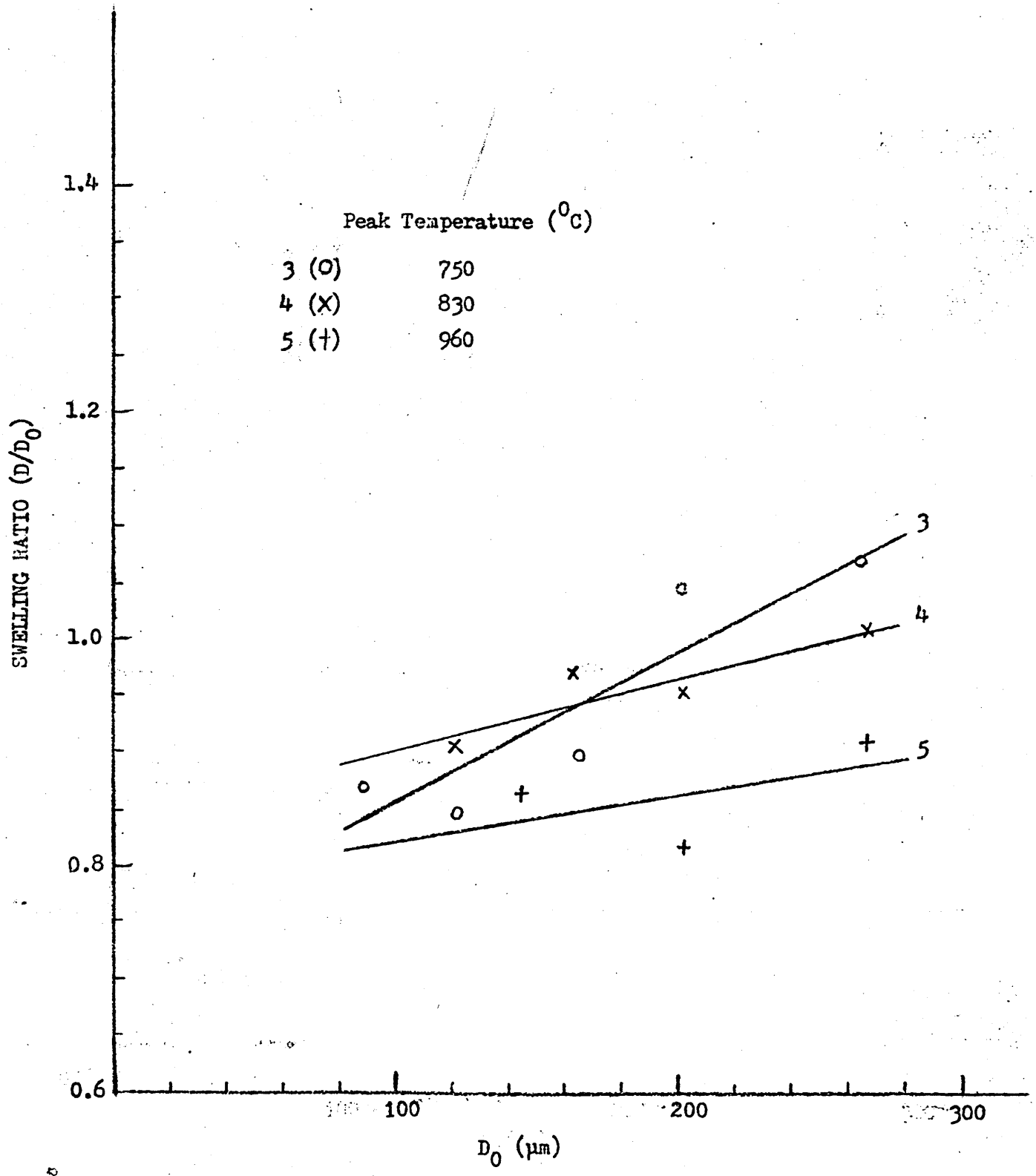

Figure 5-1b Relationship between swelling ratio and particle size

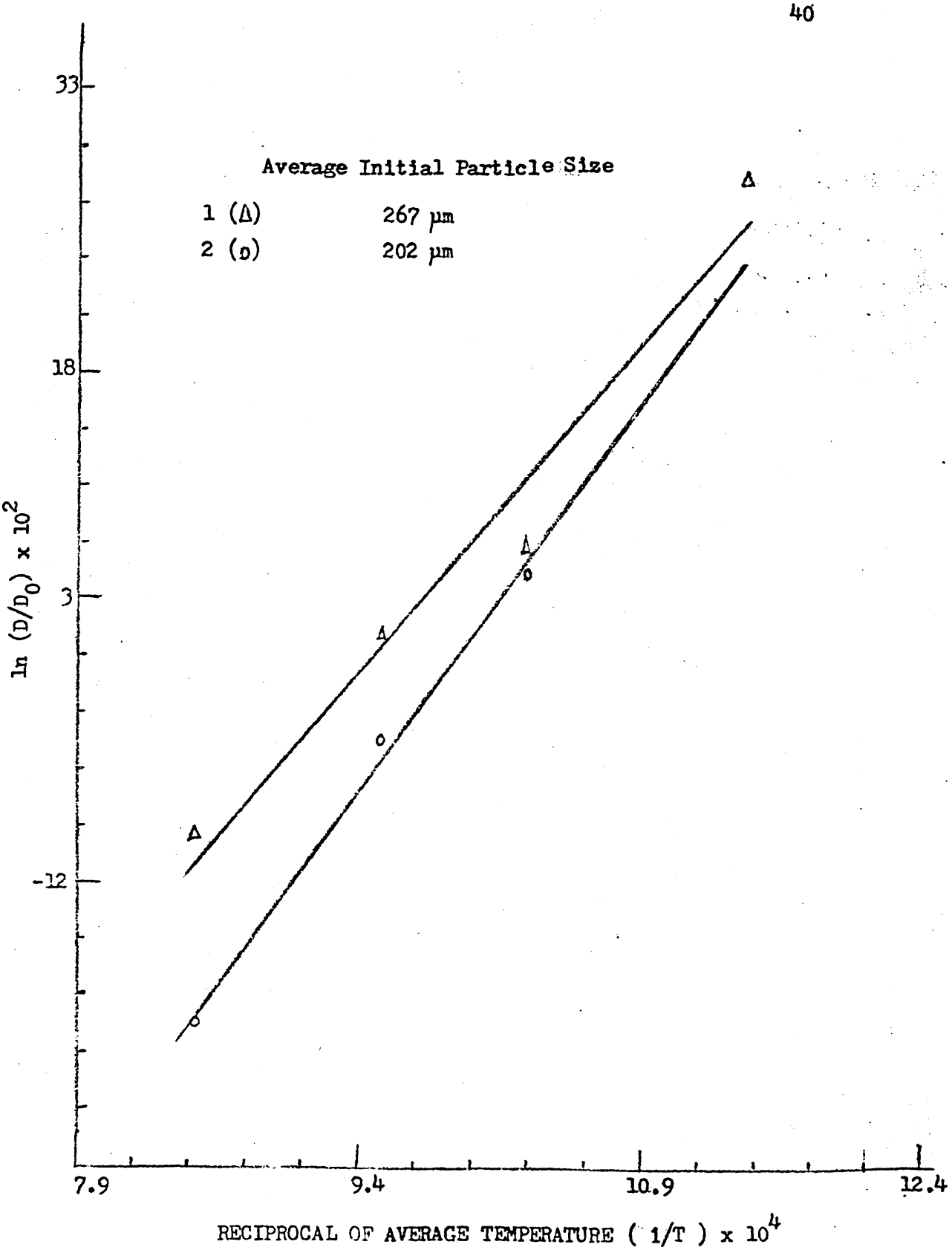

Figure 5-2a Relationship between swelling ratio and average temperature

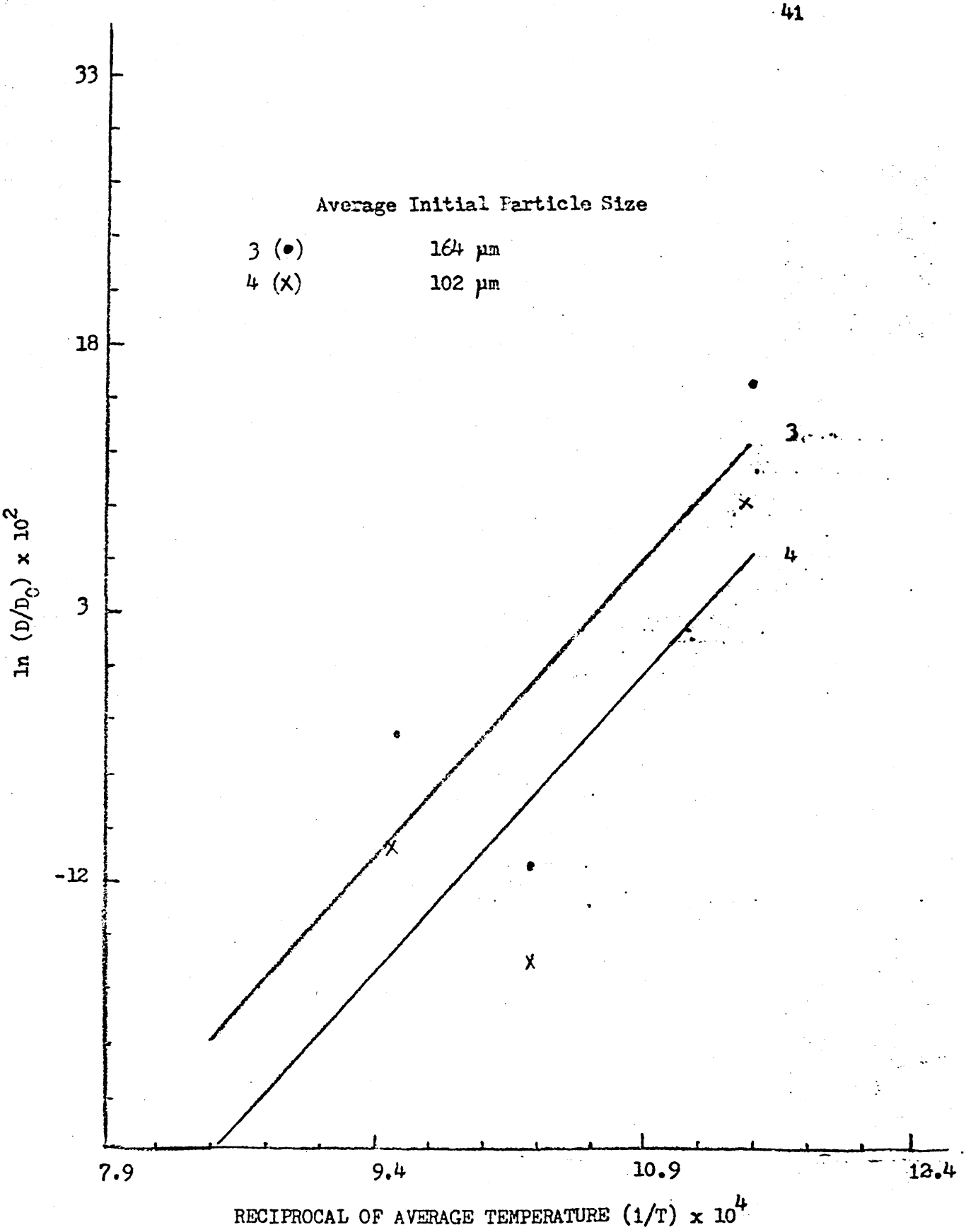

Figure 5-2b Relationship between swelling ratio and average temperature

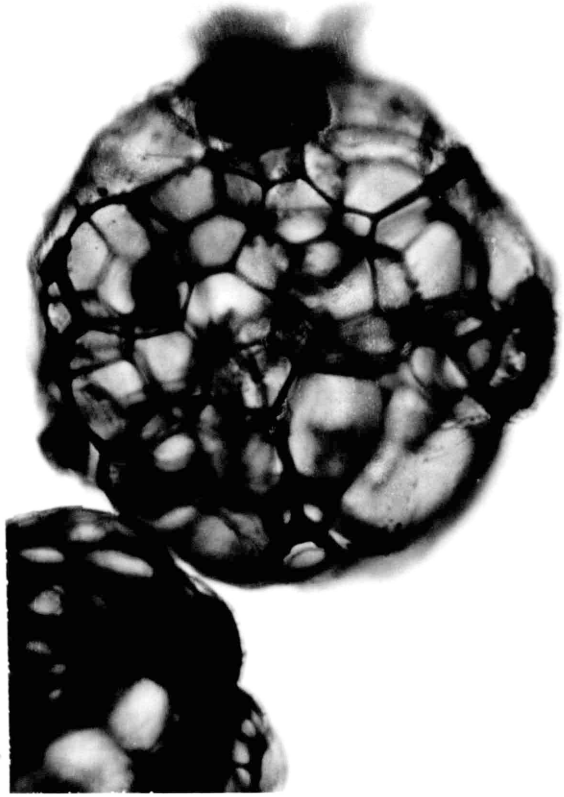

Figure 5-3a Cenosphere (10X)
Showing the ribbed window structure.

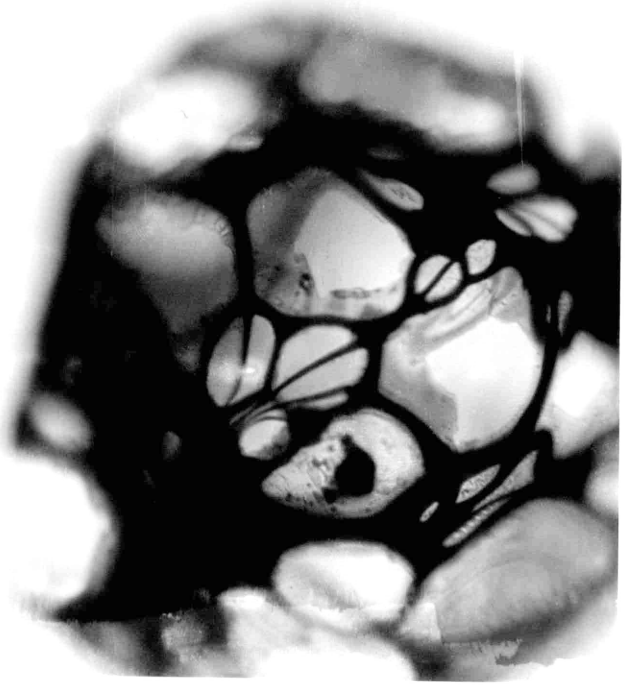

Figure 5-3b Cenosphere (10X)
Showing window destruction as a result of benzene treatment.

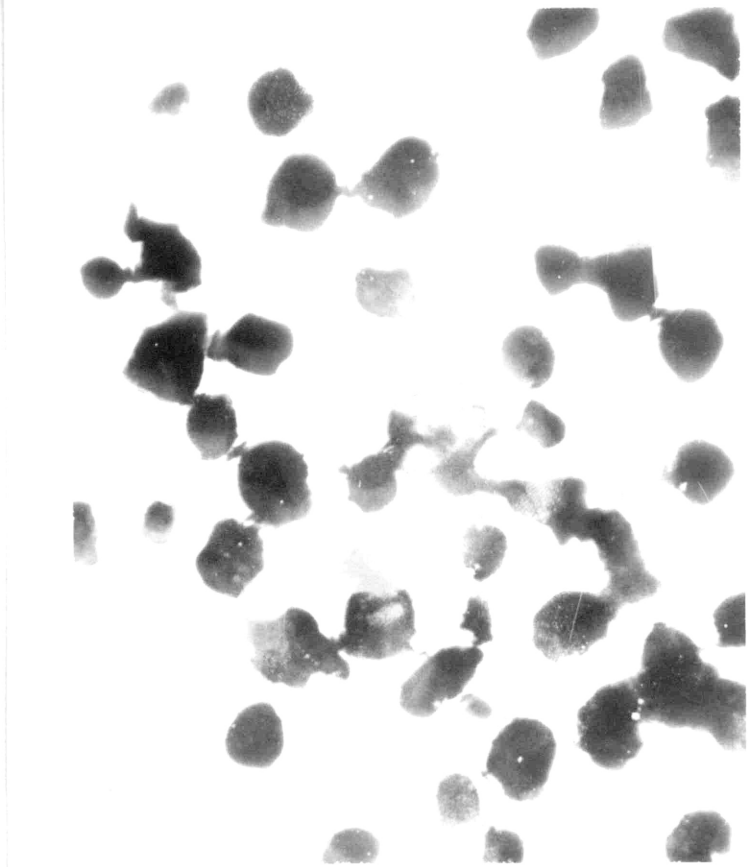

Figure 5-4a Char particles formed at 650° C.

Showing the coating at the surface of char particles and tar droplets.

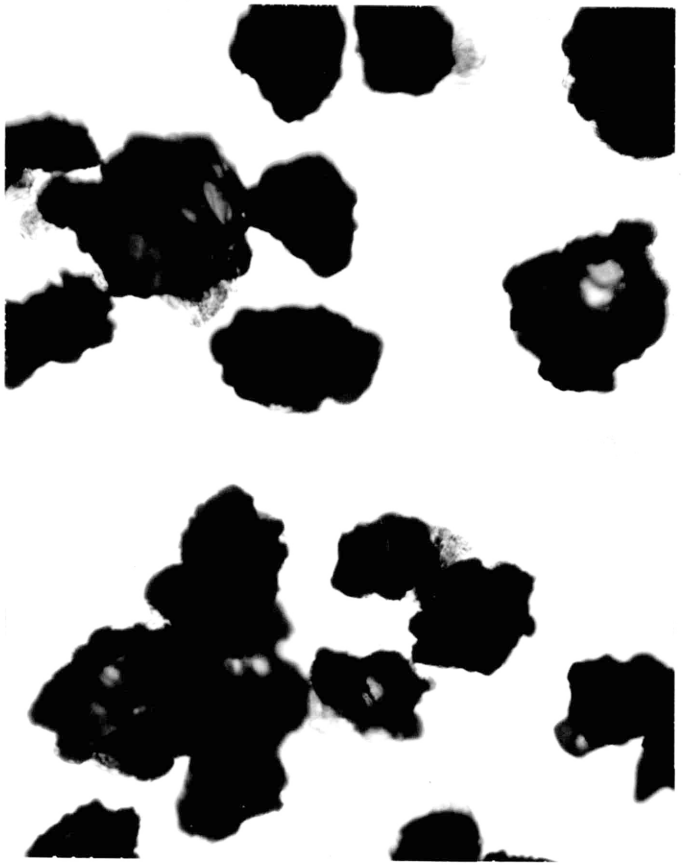

Figure 5-4b Char particles formed at 750° C.

Showing tar coating at the surface of the char particles.

Figure 5-5a Char particles formed at 650° C. (D_o=89μm, 10X)

Showing possible agglomeration.

Figure 5-5b Char particles formed at 830° C. (D_o=89μm, 10X)

Showing possible agglomeration.

Figure 5-5C Char particles formed at 960° C.
(D_o=89μm, 10X)

Showing possible agglomeration.

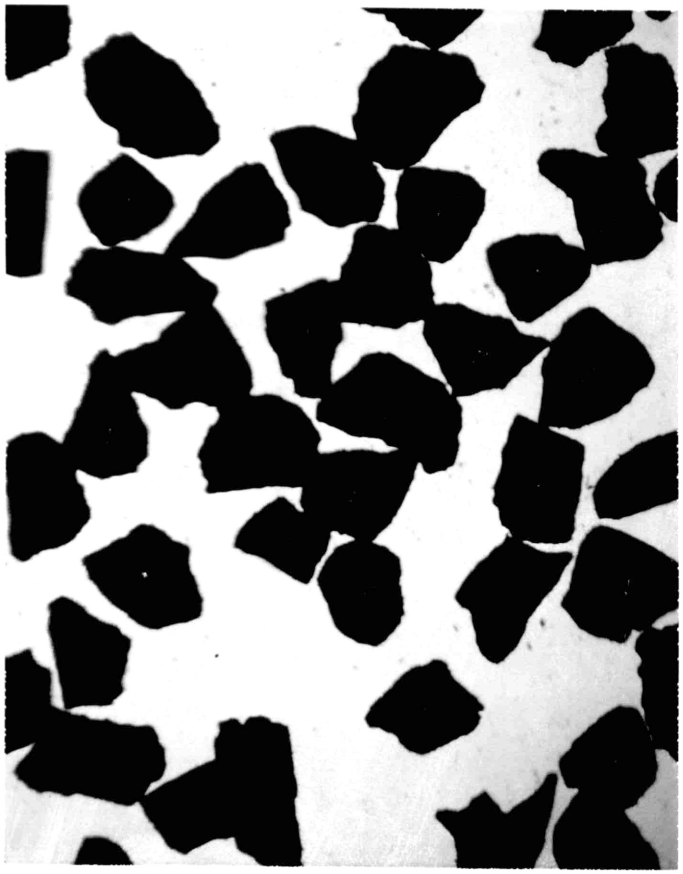

Figure 5-6a Original coal particles. (D_o=267μm, 4X)

Figure 5-6b Opaque particles and Cenospheres formed at 600° C. (D_o=267μm, 4X)

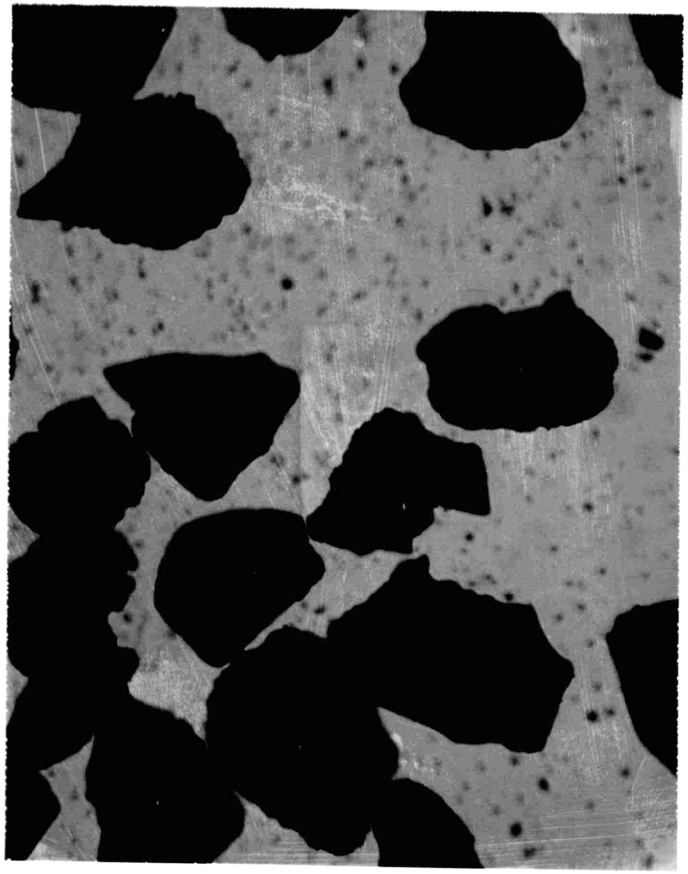

Figure 5-6c Original coal particles. (D_o=202μm, 10X)

Figure 5-6d Opaque particles formed at 600° C. (D_o=202μm, 10X)

Showing minute vesicles on the surface of the char particles.

Figure 5-6e Original coal particles. (D_o=164μm, 4X)

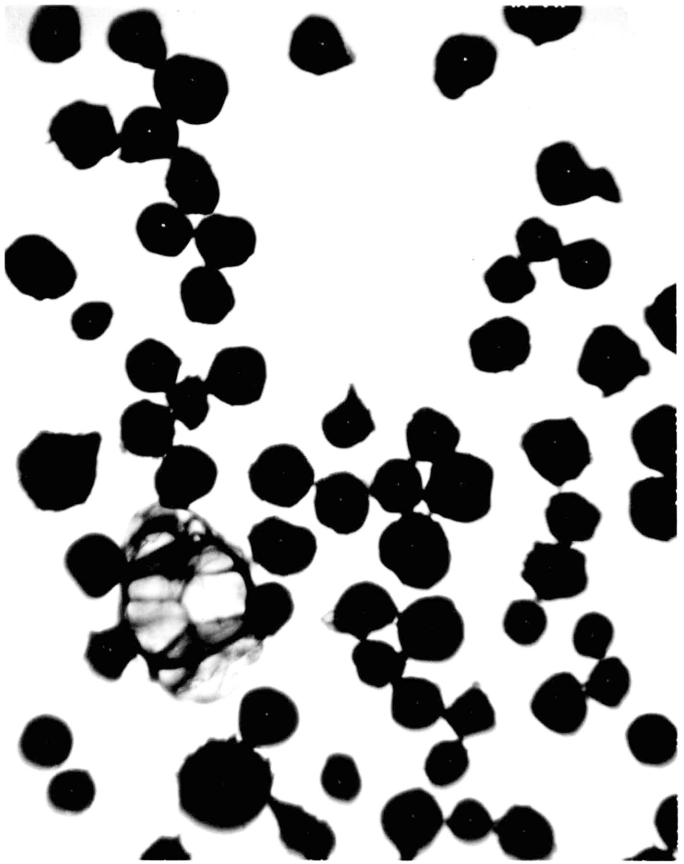

Figure 5-6f Opaque particles and Cenospheres formed at 600° C. (D_o=164μm, 4X)

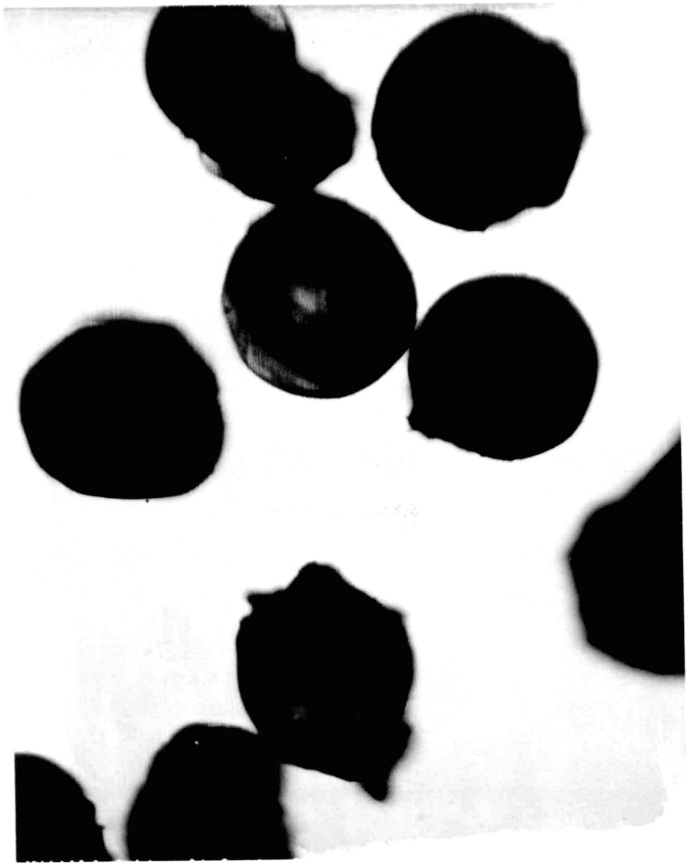

Figure 5-6g Opaque particles and cenospheres formed at 600°C. (D_o=164μm, 10X)

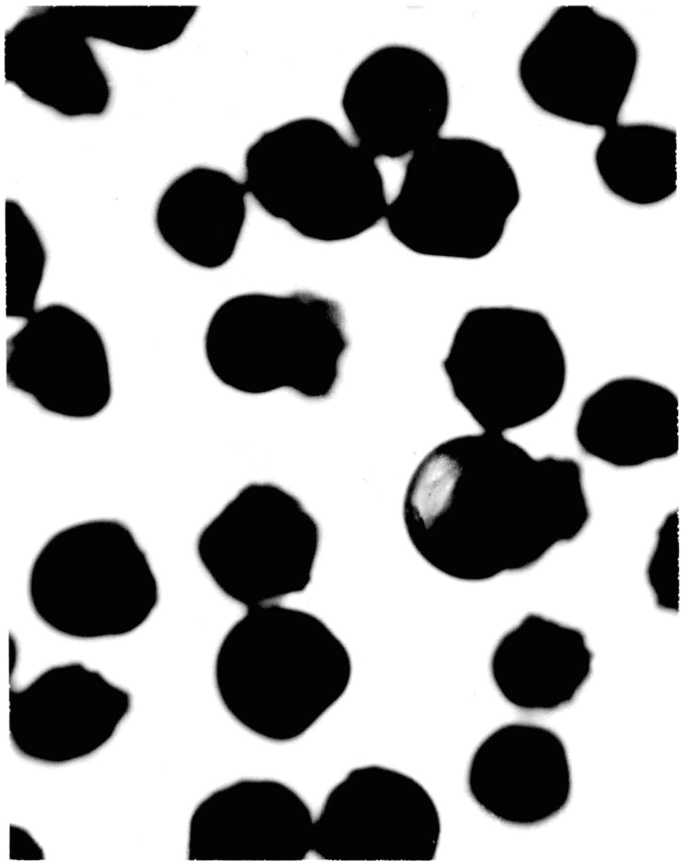

Figure 5-6h Opaque particles and cenospheres formed at 600°C. (D_o=122μm, 10X)

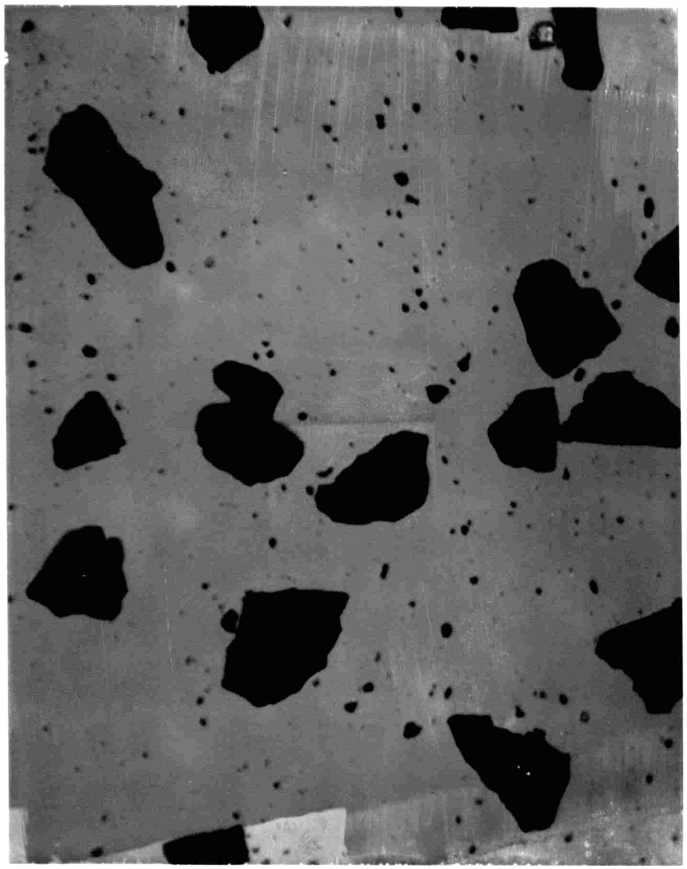

Figure 5-6i Original coal particles. (D_o=89 μm, 10X)

Figure 5-6j Opaque particles and cenospheres formed at 600° C. (D_o=89 μm, 10X)

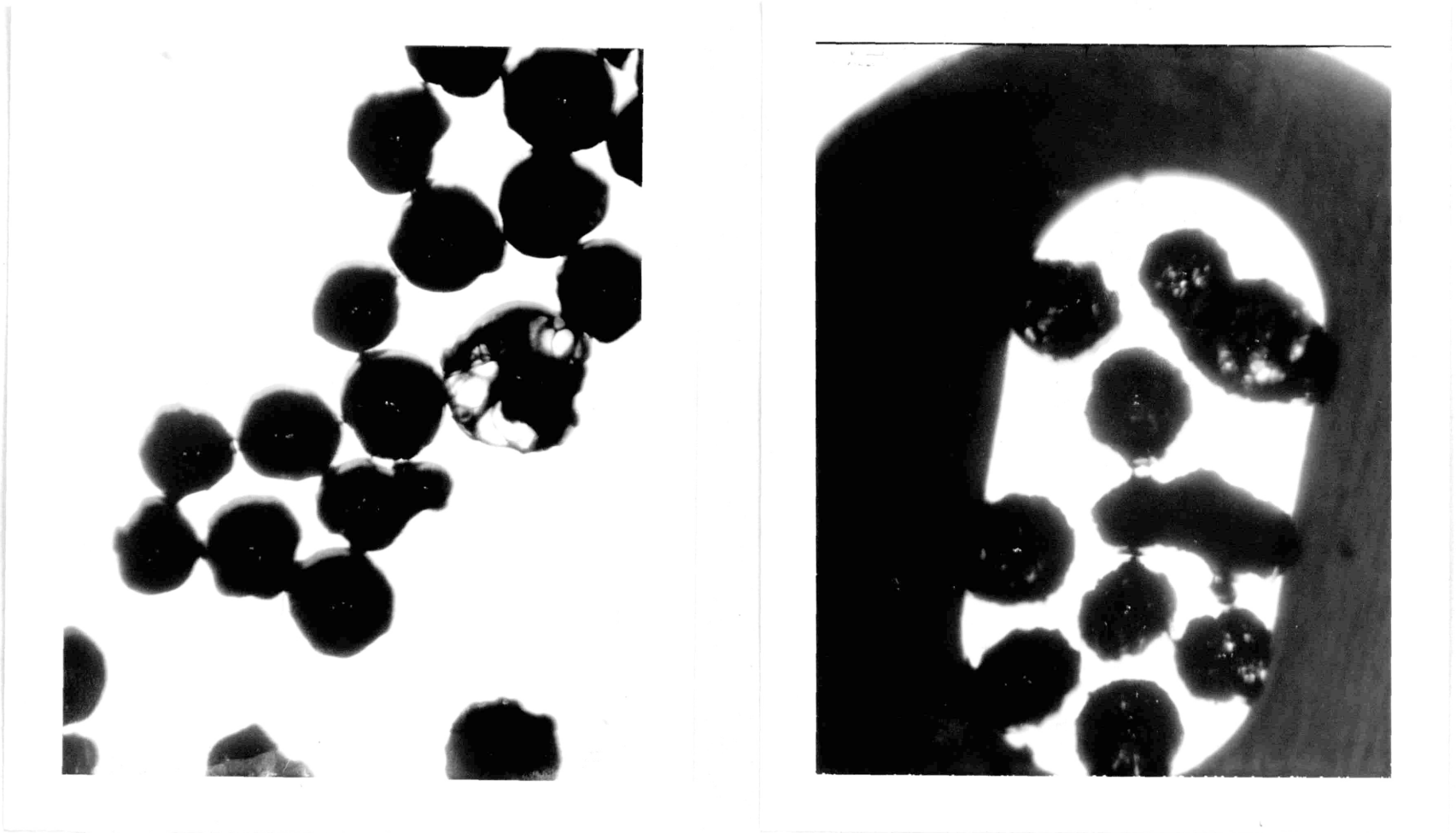

Figure 5-7a,b Opaque particles and cenospheres formed at 650° C. (D_o=267 μm, 4X)

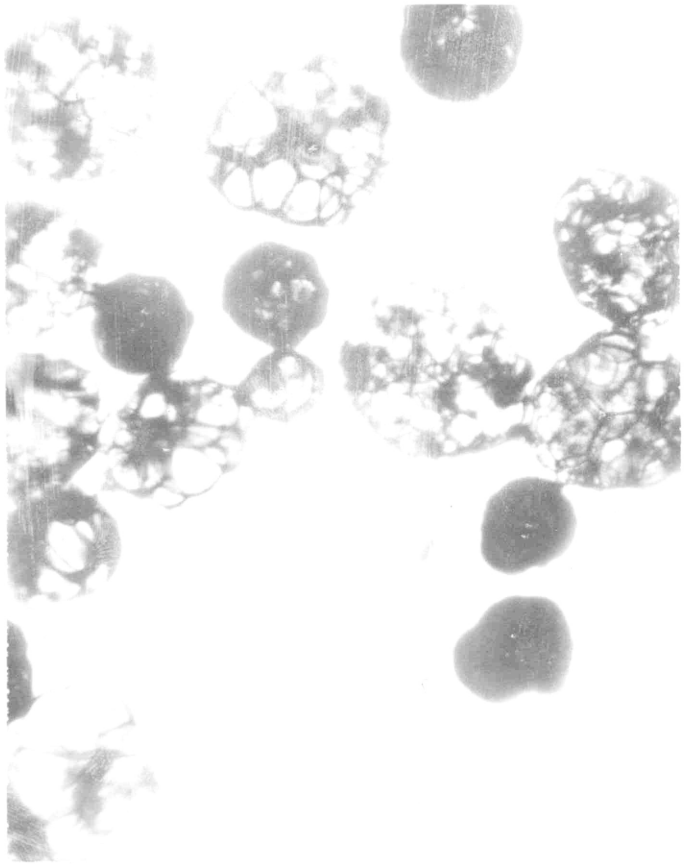

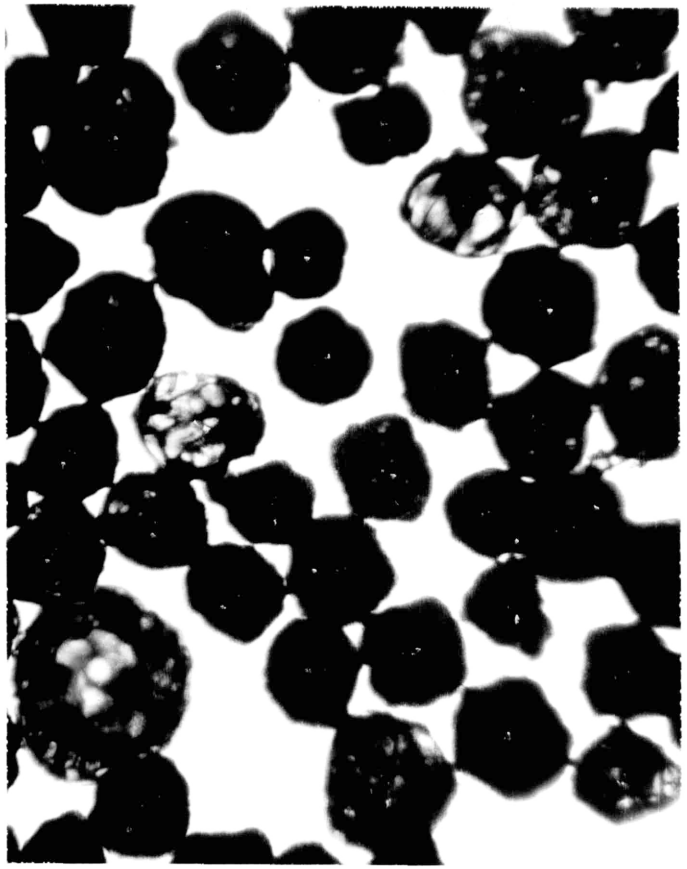

Figure 5-7c,d Opaque particles and cenospheres formed at 650° C. (D_o=202 μm, 4X)

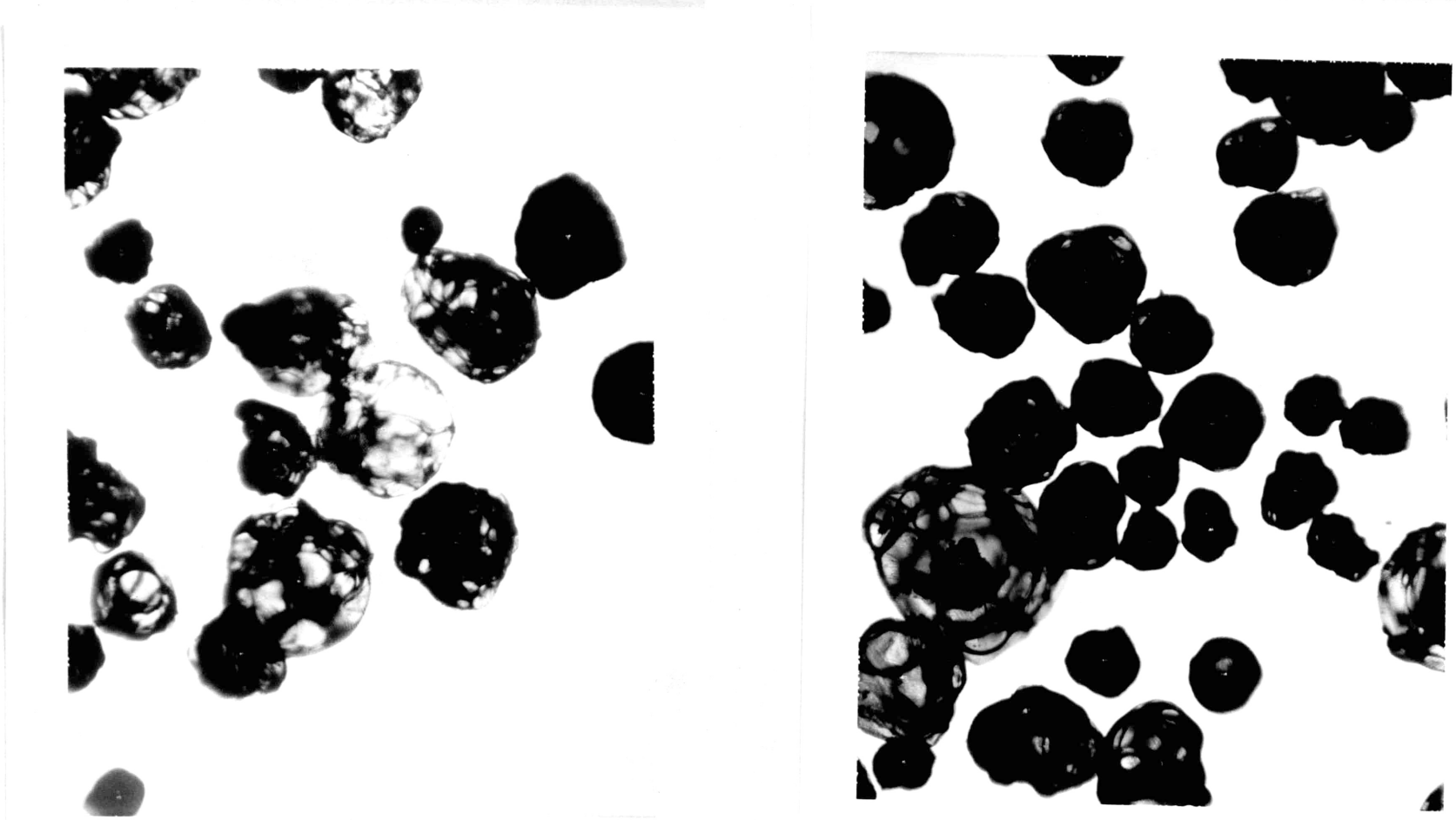

Figure 5-7e,f Opaque particles and cenospheres formed at 650° C. (D_o=164 μm, 4X)

Figure 5-7g Original coal particles. (D_o=122 μm, 4X)

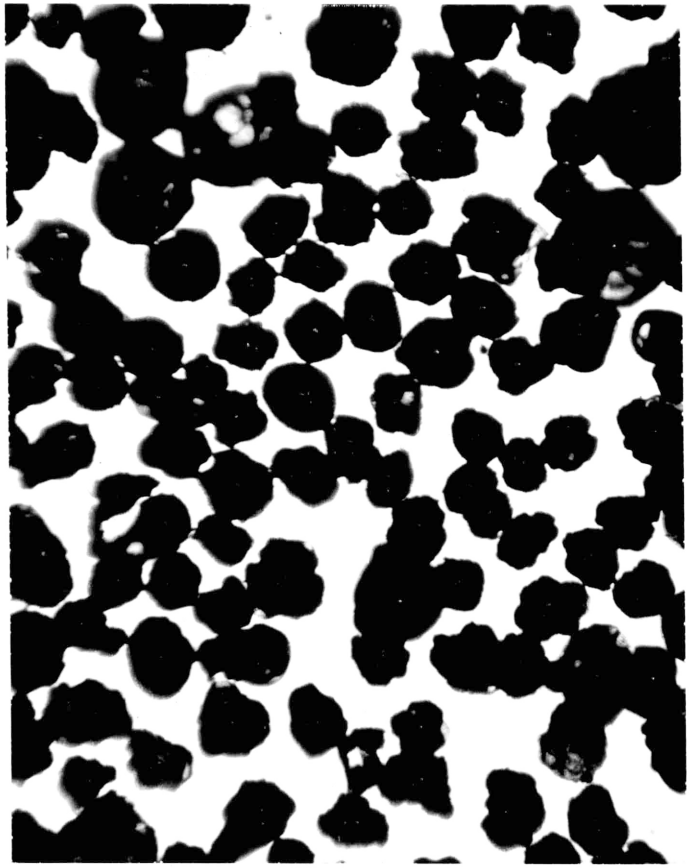

Figure 5-7h Opaque particles and cenospheres formed at 650° C. (D_o=122 μm, 4X)

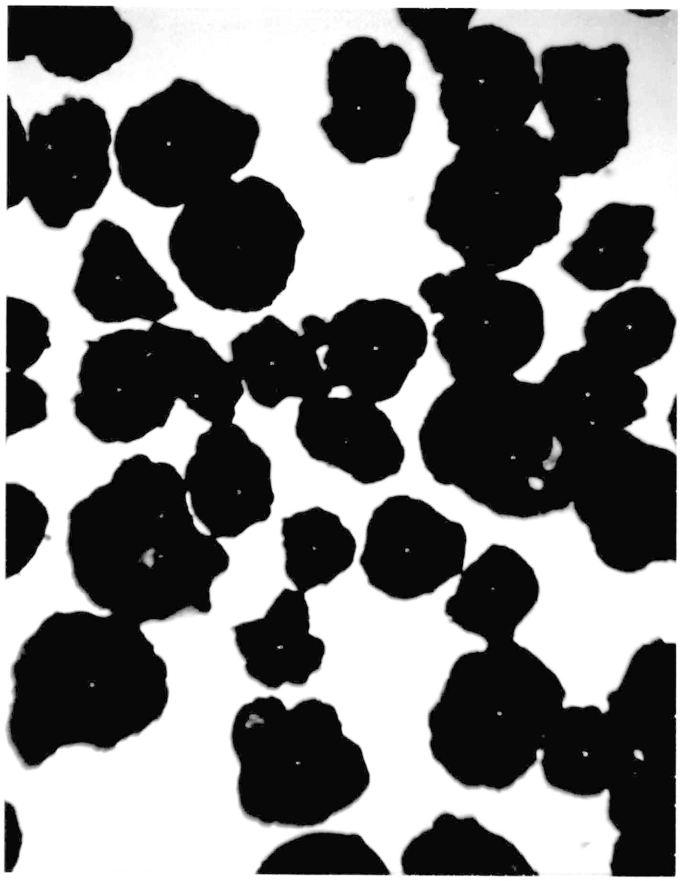

Figure 5-8a Opaque particles and cenospheres formed at 750° C. (D_o=267 μm, 4X)

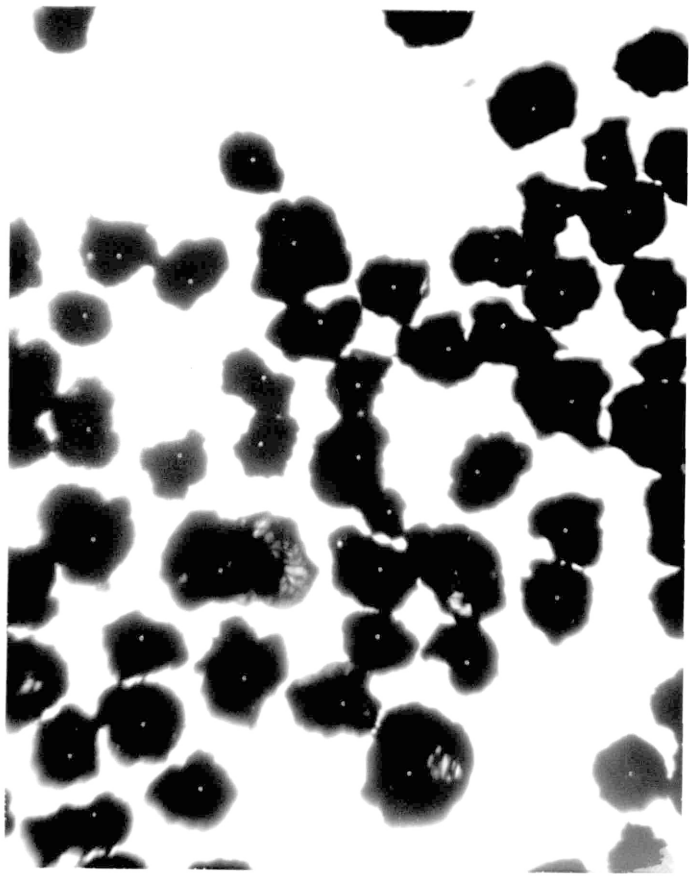

Figures 5-8b,c Opaque particles and cenospheres formed at 750° C. (D_o=202μm, 4X)

Figure 5-8d Opaque particles and cenosphere formed at 750° C. (D_o=164μ m, 4X)

Figure 5-8e Opaque particles and cenospheres formed at 750° C. (D_o=122μ m, 4X)

Figure 5-9a Opaque particles and cenospheres formed at 830° C. (D_o=267 μm, 4X)

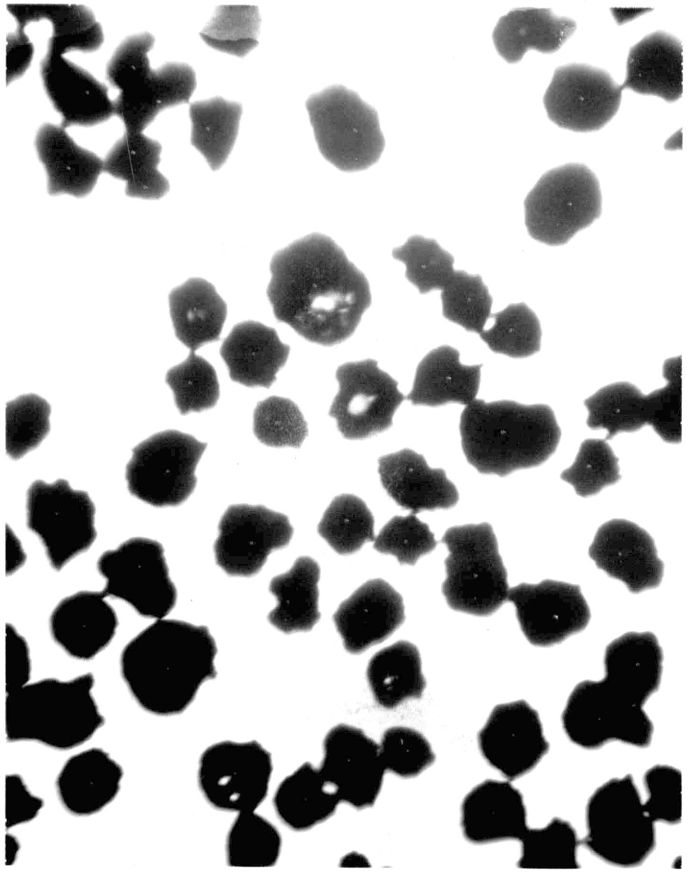

Figure 5-9b Opaque particles and cenospheres formed at 830° C. (D_o=202 μm, 4X)

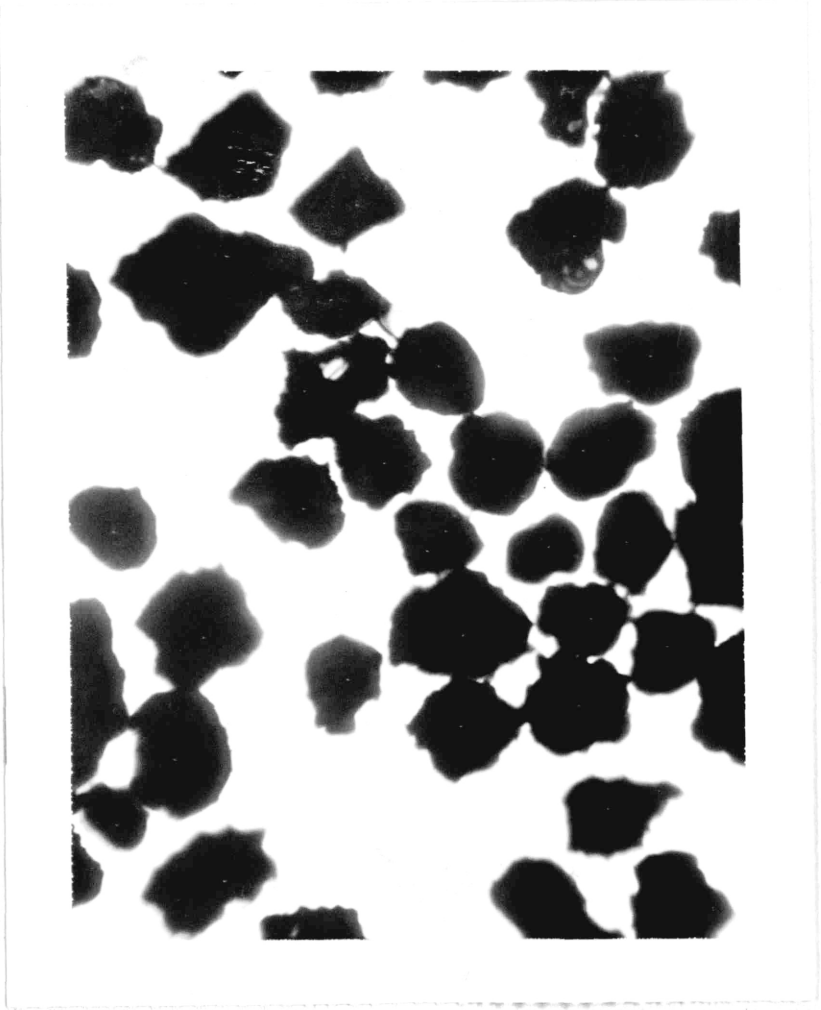

Figure 5-9c Opaque particles and cenospheres formed at 830° C. (D_o=164μm, 4X)

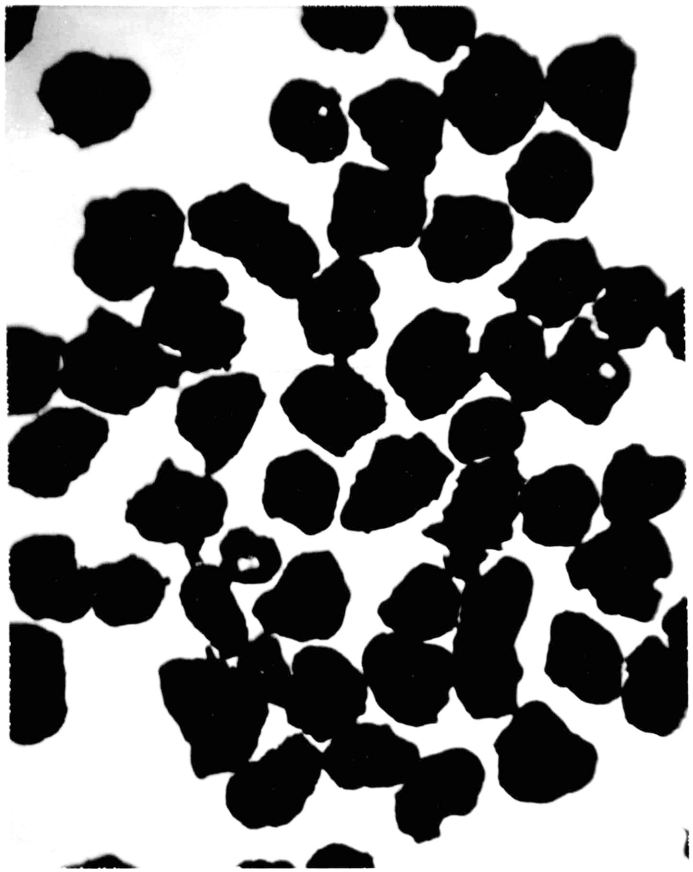

Figure 5-10a Opaque particles and cenospheres formed at 960° C. (D_o=267 μm, 4X)

Showing open and closed window structure.

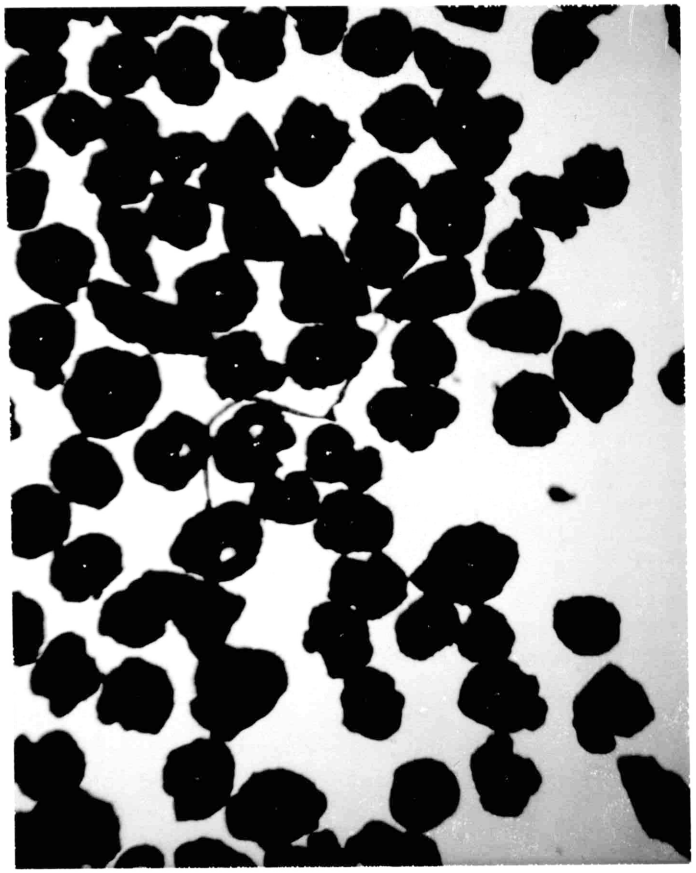

Figure 5-10b Opaque particles and cenospheres formed at 960° C. (D_o=202 μm, 4X)

Showing open and closed window structure.

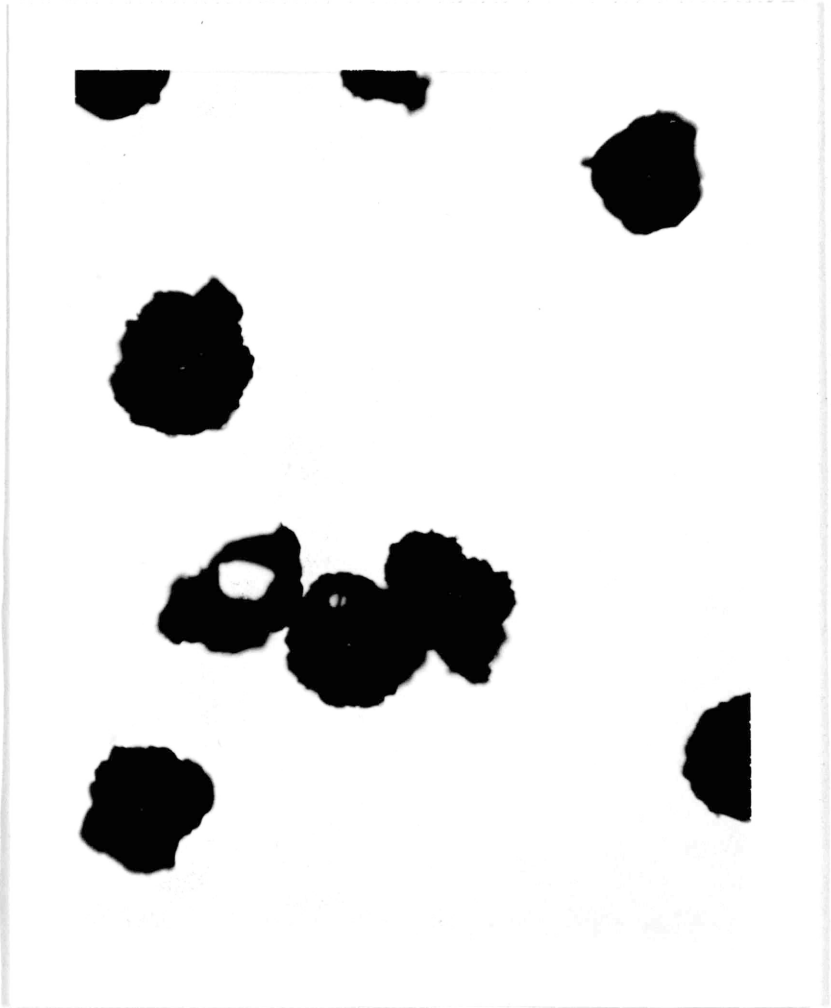

Figure 5-10c Cenospheres and char particles formed at 960°C. (D_o=122 μm, 4X)

Showing open and closed window structure.

Figure 5-11a Original coal particles. (D_o=41μm, 10X)

Figure 5-11b Agglomerating opaque particles formed at 600° C. (D_o=41μm, 4X)

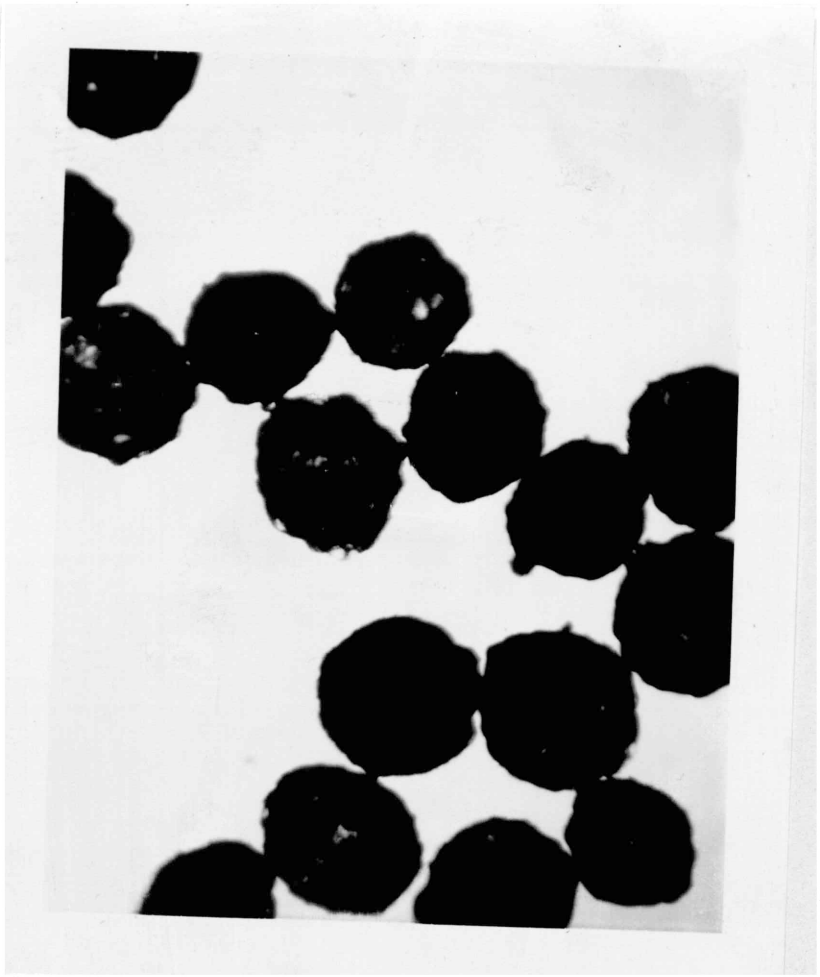

Figures 5-11c,d Agglomerated opaque particles and cenospheres formed at 650° C. (D_o=41 μm, 4X)

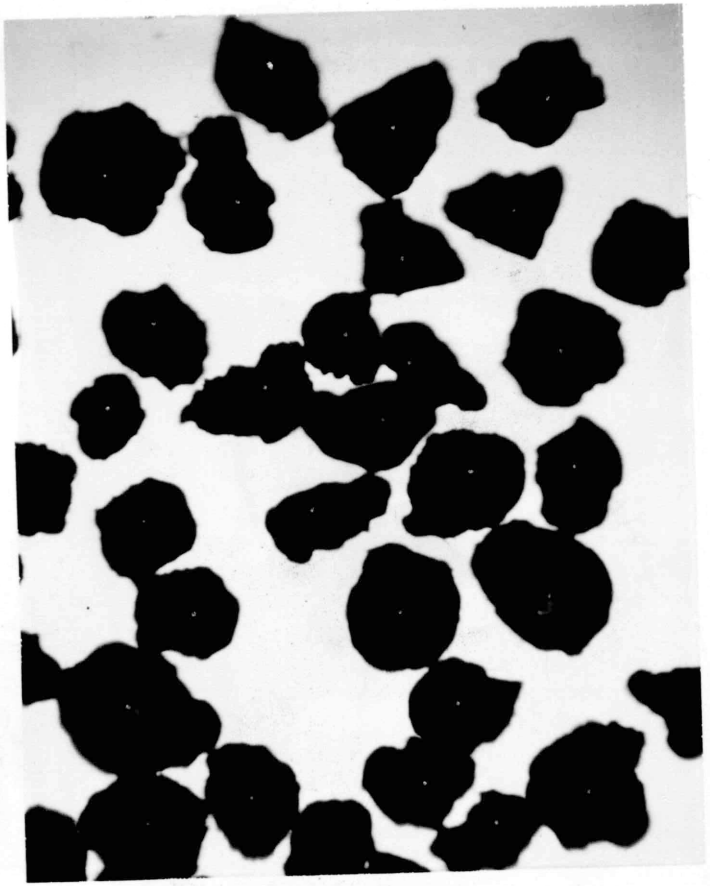

Figure 5-11e Agglomerated opaque particles and cenospheres formed at 750° C. (D_o=41 μm, 4X)

Figure 5-11f Agglomerated opaque particles and cenospheres formed at 830° C. (D_o=41 μm, 4X)

Figure 5-11g Agglomerated opaque particles and cenospheres formed at 960° C. (D_o=41μm, 4X)

6. DISCUSSION

6.1 Error Analysis

6.11 Determination of Particle Size

The greatest possible source of error in determining the swelling ratio of char particles comes from the assumption that each coal particle has uniform cross sectional area for all possible orientations, i.e. a sphere, A large portion of coal particles counted had random configurations, therefore the assumption is not very good. The situation can be improved if a large number of particles of a narrow particle size distribution is used. It is hoped that by counting a large number of particles, all possible particle cross sectional areas are covered so that the average of them is the representative cross sectional area of the particles when the particles assume a spherical configuration.

The measuring process employed using TZG 3 has several possible sources of error. The most important one is the error in matching the area of a circular iris with the area of a noncircular particle image by equating the area of the particle image outside the iris with the area inside the iris not convered by the particle image. The equating process is purely dependent upon personal judgement, thereby making consistency and care essential in the process of measuring. Hopefully, by employing a large number of particles in size counting, the errors will cancel each other. To test the consistency of the process, several particle sizes were measured twice, and it was found that the average particle sizes differed by 2 μm to

5 μm. Other errors introduced in this measuring process involved the sensitivity of the TZG 3. It was mentioned earlier that the counter number of TZG 3 was calibrated using a magnified reference scale. For the operation of the standard linear distribution curve, the sensitivity of the counter number is 12 μm and 4 μm for maginification of 4 X and 10X respectively. For the operation of the reduced linear distribution curve, the sensitivity of the counter number is 4 μm and 1.6 μm for magnification of 4X and 10X respectively. Since the standard linear distribution curve for 4X has an error of 12 μm in counting, it was used only for particle sizes greater than 200 μm.

6.12 Constant Residence Time And Heat Transfer Limitation

Constant residence time for all particle size distributions of interest is required. This can be accomplished by using a constant main gas velocity in the laminar flow region above the final settling velocity of the coal particles, so that the coal particles will travel down the reaction tube with the main gas at approximately equal velocity. The flow rate of the main gas was adjusted for different peak temperatures to achieve a constant main gas velocity. In this study, it was assumed that all particle sizes of interest traveled down the reaction tube with a velocity of 2 ft/sec, which is the velocity of the main gas. To determine the validity of the assumption, final settling velocities for initial coal particle sizes of 270, 200 and 180 μm were calculated for temperatures of 600°, 700°, 800° and 900 °C using Stoke's Law and the Ladenburg wall correction factor. It was found that the final particle settling

velocities were greater than the main gas velocity for particle sizes greater than 200 μm. (See Appendix A-6). For the particle size of 270 μm, the final settling velocity exceeds the main gas velocity by a factor of 1 to 0.5; therefore, the residence time for an average particle size of 267 μm is probably smaller than 1/3 second. The higher value of the final particle settling velocity than of the gas velocity has an important effect on the particle temperature. The main concern here is the development of an effective thermal boundary layer which is higher than the effective thermal boundary layer of a stagnant flow due to a difference between the gas and the particle velocity. As the effective thermal boundary layer increases because of increasing particle size and deviation from stagnant flow, the temperature of the particles will decrease and deviate from the main gas temperature. Since there is no direct way of measuring the particle temperature, the extent of the temperature deviation from that of the main gas due to non-stagnant flow and large particle size can not be determined. But a hint of the existence of the greater temperature deviation from the main gas due to non-stagnant flow and large particle size can be obtained by examining the char products of different size distributions collected at the same peak temperature. It was discovered that, at a peak temperature of 600°C, char products of the initial average particle size of 267 μm were not round although the rest of the char products were round. (See Figure 5-6b,d) The difference is probably due to the incomplete fusion of char products of the initial average particle size of 267 μm because of

a lower particle temperature.

6.2 Treatment of Tar Condensation on Char Products

The experimental procedure for the preparation of particle images of char particles formed at the peak temperature of 650°C differed from the preparation of the rest of the char samples because condensation of tar occured at the surface of these particles.

Before char products were examined under the microscope, it was noticed that the color of the inside wall of the ceramic vial became more intense than its original color (light brown) at the end of each run for peak temperatures of 650°C and 750°C. But the intensity of the color decreased as the peak temperature went up to 830°C. At the peak temperature of 960°C and 600°C, the color of the inside wall of the ceramic vials remained the same. It was also observed that the char particles produced at the peak temperatures of 650° and 750°C had a greater tendency to stick to the ceramic wall than other char products formed at the peak temperatures of 600°, 830° and 960°C. A microscopic examination of the char particles formed at the different peak temperatures revealed that at 650°C, some particles were coated with a dark brown, tar-like substance, and that tar droplets were present in the samples. (See Figure 5-4a). The coating of tar at the surface of the particles was less intense at the peak temperature of 750°C. (See Figure 5-4b). At 600°, 830° and 960°C, there was little or no visible tar coating at the surface of the particles. (Nearly all char samples collected had a very thin layer of film which could not

be detected under the microscope. The presence of this thin film was demonstrated by the diffraction effect observed under the microscope.) Most of the tar coating was one sided at the surface of the particles. This was explained as caused by tar condensation in the main gas upon cooling. When the main gas carried the evolved tar to the ceramic vial through the water-cooled sample probe, it condensed out and then deposited at the surface of the particle, the surface of the ceramic vial and the wall of the water-cooled sample probe. As the temperature increased, the amount of tar present in the main gas increased due to a greater extent of thermal decomposition of coal at a high temperature. So when the main gas was cooled, the amount of tar condensed also increased with temperature. But when the temperature increased to a certain point, the cracking of tar to solids and gases started to take place, and therefore the amount of tar present in the main gas decreased. So when the main gas was cooled, the amount of tar condensed decreased as the rate of tar cracking increased with temperature. Lau (1977) experimented with cracking of propane in the laminar flow reactor. He observed that the cracking of propane started to take place at the peak temperature of 750°C, and that the amount of propane being cracked increased with an increase in the peak temperature. When the peak temperature reached 960°C, 98% of the original material was cracked. His observed cracking phenomena coincided well with the observed tar condensation phenomena at the surface of the char particles.

Since some of the condensed tar at the surface of the char particles formed at the peak temperature of 650°C was dark brown, the

distinction between the char phase and tar phase could not be readily detected in the particle images. For fear of interference of condensed tar during size counting, it was decided to suspend the char particles formed at the peak temperature of 650°C in a benzene solution on a microscope slide to wash out the tar. Then they were dried carefully before photographing. The only concern of this method was the possibility of destruction of cenospheres, but it was found that the cenospheres did not disappear when a few drops of benezene were carefully added to them Sometimes, however, the window structure was dissolved partially if too much benezene was added. (See Figure 5-3b). Since the tar condensation at the peak temperature of 750°C was not significant and less intense in color, the benzene treatment was not applied to them.

6.3 Structure of Coal Residue

Although the physical structure of coal is complex, when the particles were examined under the light microscope, no complexity was observed. Most coal particles examined were opaque under the light microscope of TEM 200, but they were a few exceptions. It was observed that less than 1 % of the coal particles examined appeared to be either dark brown or silver under the light microscope. The dark brown particles were suspected to be mostly tar, and the silver particles to be metal. The silver particles did not appear to go through any physical change under these experimental conditions.

The structure of the char products appeared to be more heterogeneous than the original coal particles. The heterogeneity wa

caused by the fact that portions of coal particles were transparent. A microscopic examination of unagglomerated char products formed at the temperature of 600°C revealed the occurence of transparent coal particles, the formation of cenospheres. (See Figure 5-6b,f,g,h,j). But the number of cenospheres which could be detected under the light microscope at this peak temperature was not significant. On the average, fewer than 5% of the particles examined had detectable ribbed window structures, and even a fewer number of cenospheres had the distinct ribbed window structure as shown in Figure 5-3a. Cenospheres having the distinct ribbed window structure usually exhibited a much larger increase in volume than the average char particles. (See Figure 5-6f). Most of the particles were opaque and round, and some had minute vesicles at their particle surface. (See Figure 5-6d). But, for the initial average particle size of 267 μm, most of the particles were not round. There was some swelling at this peak temperature, but it was not very significant. (See Figure 5-6a, b, c, d, e, f, i, j).

Char particles of agglomerated coal particles appeared similar to unagglomerated coal particles, namely, round and opaque. There were no cenospheres detected for agglomerated coal particles. (See Figure 5-11b).

When the peak temperature increased to 650°C, the most drastic change in char products was a significant increase in the number of cenospheres detected. Most of the cenospheres formed had distinct ribbed window structures. The size of cenospheres and windows also increased. (See Figure 5-7a, b, c, d, e, f, h). The formation of cenospheres was most

significant at the initial particle size of 202 μm. More than half of this sample had detectable ribbed window structures. This is a much higher percentage than that of the rest of the char sample formed at this peak temperature. On the average, approximately 30 % of the char particles had detectable cenospheres. It is difficult to conceive of an explanation for the significant difference. It is probably due to experimental errors, i.e., the peak temperature was off for this particular run. Most of the particles were spherical, and there were also minute vesicles at the particle surface. The swelling of the particles at this peak temperature appeared to be more significant than the char particles formed at the peak temperature of 600° C. Both agglomerated and unagglomerated char particles behaved similarly at this peak temperature. (See Figure 5-11c, d)

At a temperature of 750° C, the formation of cenospheres was observed. But, the number of cenospheres that could be detected was reduced, and the sizes of cenospheres were also reduced. (See Figure 5-8a, b, c, d, e). There was an increase in the opacity of particles. Approximately 10 % of the char products had detectable ribbed-window structures at this peak temperature, but there were no cenospheres behaving like the one shown on Figure 5-3a. Most char particles formed were not as round as char particles formed at the peak temperature of 650°C. Miinute vesicles could still be detected at this peak temperature. Both agglomerated and unagglomerated char particles behaved similarly. (See Figure 5-11e). The shrinking

of the unagglomerated char particles was observed at this peak temperature.

When the peak temperature reached 830° C and 960° C, most of the particles were opaque. There were no detectable particles behaving like the one shown in Figure 5-3a. At the peak temperature of 830° C, a small portion of the char particles had ribbed window structures. (See Figure 5-9a, b, c). At the peak temperature of 960° C, some of the ribbed window structures were open, i.e. there were continuous pores. (See Figure 5-10a, b, c). Minute vesciles could also be detected at these two peak temperatures. The agglomerated and unagglomerated char particles behaved similarly at these two temperatures. The unagglomerated char particles formed at these two peak temperatures were smaller than the original coal particle.

In brief, the detection of the cenospheres was highly temperature dependent under the employed experimental conditions. The trend observed in this study coincided with Newall and Sinnatt's observation. (See Section 3.3). The number of cenospheres detected and the size of cenospheres peaked with a certain temperature. The exact point of the maximum detection of cenoshperes is not known at present, but it is suspected to be in the peak temperature range of 600° C to 750° C.

The minute forms observed by Newall and Sinnatt (1924) could not be detected under the light microscope since the magnification used in this study was not high enough.

6.4 Relationship Between Swelling Ratio And Particle Size

Table 5-1 shows the effect of particle size on the average swelling

ratio at the constant peak temperature for all particle size distributions employed in thestudy. The data here do not always show an increase in the swelling ratio of char samples free of agglomeration with an increase in particle size. But it is reasonable to conclude that the swelling ratio increases with an increase in particle size. The relationship between the swelling ratio and the initial particle size predicted by Lewellen (1975) is nearly linear with the initial particle size in the range of 120 μm to 230 μm. (See Figure 3-9). Data analysis of swelling ratio vs. particle size at constant peak temperature was performed for samples that were free of agglomeration. The least square method was used for this analysis. The results are tabulated in Table 5-2 and the graphical results are presented in Figure 5-1a and 5-1b. It is interesting to note that the slopes of D/D_0 vs. D_0 for peak temperatures of 600°, 650° and 750° C were very similar to that of Lewellen's particle size trend prediction (1.6×10^{-3}). The experimental conditions employed in this study were not similar to that of Lewellen's simulation, so the significance of the coincidence is uncertain. The slope of the curve decreases as the peak temperature increases. This implies that, at the high peak temperature, the particle size has less effect on the swelling ratio. Curve 3 and Curve 4 on Figure 5-1b intersect at 165 μm. This is unlikely and it is probably caused by the scattering of data. In general, the linear relationship between the swelling ratio and the particle size fits the data well. The deviation of data from the corresponding value determined by the least square method is within 5 % of its corresponding value. There are a few exceptions which have approximately

10 % deviation.

Due to particle agglomeration, no accurate data were obtained for initial average particle sizes less than 89 μm. But it is expected that the swelling ratio will be nearly constant for very small particle sizes since the bubbles generated inside the coal particle will be instantaneously transported to the surface and escape.

According to Lewellen's study (1975), the swelling ratio will not increase linearly with particle sizes above 230 μm. The increase in swelling ratio with the initial particle size will be less significant as the particle size increases above 230 μm. Since not enough experiments have been done for average particle sizes greater than 230 μm, the validity of Lewellen's predicted trend remains uncertain.

6.5 Relationship Between Swelling Ratio And Temperature

Table 5-1 also shows the effect of temperature on the average swelling ratio of unagglomerated char particles at the constant initial average particle size. The table shows that the swelling ratio peaks at the peak temperature of 650° C. The swelling ratio increases with the peak temperature when the peak temperature increases from 600° C to 650° C, and peak temperature of 650° C. Increasing the peak temperature from 600° C to 650° C always increases the swelling ratio; in most cases however, increasing the peak temperature from 650° C to 960° C causes a decrease in swelling ratio. The observed trend agrees well with the predicted trend discussed in Section 3-6. The swelling-temperature relationship is similar to the thermal decomposition rate-time-temperature relationship in pyrolysis, i.e. both peak at a certain temperature. It was decided to correlate $\ln(D/D_o)$ with 1/T (reciprocal of the average temperature of the reactor) at a constant

initial particle size. The average temperature range for the correlation was 600°C to 900°C. The least square method was used for this correlation. The results of the correlation are tabulated on Table 5-3, and plotted in Figure 5-2a, b. As is evident from Figure 5-2a, a linear relationship exists between the $\ln(D/D_0)$ and $1/T$ at the initial particle sizes of 267 and 202 μm. But the correlation was not satisfactory for the initial particle sizes of 164 and 122 μm. This is probably due to errors in size counting or scattering of data. Since insufficient data were obtained to draw any correlation between the swelling ratio and the average temperature for average temperatures below 600°C, the empirical relationship between the swelling ratio and the temperature is still undefined.

There were two assumptions made in correlating the swelling ratio with the average temperature. First, the nonuniformity of heating rate at different average or peak temperatures has little or no effect on the swelling property of the coal samples. Secondly, the average or peak temperature of the reactor corresponding to the maximum swelling ratio does not lie in the average temperature range of 600°C to 700°C. Since the assumptions were not tested experimentally, the validity of the above correlation is still uncertain. But in general, the swelling-temperature relationship is similar to the thermal decomposition rate-time-temperature relationship or the fluidity-time-temperature relationship in pyrolysis of bituminous coal.

6.6 Agglomeration

Although the swelling ratio of agglomerated char particles displays a maximum at the peak temperature of 650°C, it does not necessarily suggest that the agglomeration of coal is temperature dependent. Since the agglomeration of char particles is caused mainly by the agglomeration of raw coal particles before entering the reactor tube, the effect of the peak temperature of the reactor on the agglomeration of char particle should be insignificant. The maximum swelling ratio observed at the peak temperature of 650°C is probably due to the more intensive swelling of agglomerated coal particles at the peak temperature of 650°C than that of agglomerated coal particles at other temperatures. It is evident from Table 5-1, that the extent of agglomeration of char particles increases as the particle size decreases. No correlation has been made to establish the relationship between the extent of agglomeration and the particle size in this study.

7. CONCLUSION

1. At constant peak temperature, the swelling ratio increases with the average initial particle size. A linear relationship can be used to describe the relationship between the swelling ratio and the initial particle sizes of 89 μm to 267 μm.

2. At constant initial average particle size, the swelling-temperature relationship is similar to the thermal decomposition rate-time-temperature relationship or the fluidity-time-temperature relationship in pyrolysis of bituminous coal, i.e. swelling, fluidity and thermal decomposition rate all peak at a certain temperature. Based on the data obtained,

an empirical relationship has been developed to correlate the swelling ratio with the average temperature of the reactor. The average temperature ranges were 600°C to 900°C. But the exact correlation of swelling ratios and the temperatures is still undefined due to a lack of information on the average reactor temperature corresponding to the maximum swelling ratio, and insufficent data obtained at low temperatures.

8. RECOMMENDATION

The validity of the assumptions used in correlating the average swelling ratio with the average reactor temperature at a constant average initial particle size were not tested experimentally. Future study should first determine the average or peak temperature of the reactor corresponding to the maximum swelling ratio of coal particles, and the effect of heating rates on the swelling ratio of char particles at constant peak temperature. The peak temperature of the reactor corresponding to the maximum swelling of char particles probably lies in the temperature region near 650°C. Therefore, future study should focus on the effect of peak temperature on swelling ratio near that region. But the effect of heating rate on the swelling ratio of char particles can not be investigated in the present set up of the laminar flow reactor since there is a one to one relationship between the heating rate and the peak temperature of the reactor. (See Appendix A-5). Once the peak temperature of the maximum swelling ratio of char particles is determined, a correlation of the swelling

ratio with the average or peak temperature of the reactor can then be made at a constant initial particle size.

Besides particle size and peak temperature of the laminar flow reactor, there are other experimental variables such as pressure and reaction atmosphere which will have significant effects on the swelling ratio of char particles. Therefore, future research can also include the study of the dependence of the swelling ratio of closely size-graded bituminous coal particles on the pressure and the atmosphere employed in the reactor.

Since the extent of fresh feed agglomeration is very significant for average initial particle sizes less than 89 μm, future research should not include particle sizes less than 89 μm. The non-stagnant flow between the coal particles and the main gas is also undesirable, hence future research should exclude particle sizes which have final settling velocity greater than the velocity of the main gas at the experimental conditions of interest.

The examination of char particles under the light microscope reveals only the surface structure of the char particles; it does not provide information on the porosity inside the char particles. Future study can also focus on the study of porosity of char particles of bituminous coal formed under different experimental variable. If there is a large scale of porosity present inside the char particles, it can be detected using a refractive microscope. The char particles must be imbedded in epoxy resin and polished before examining them under a refractive microscope.

9. APPENDIX

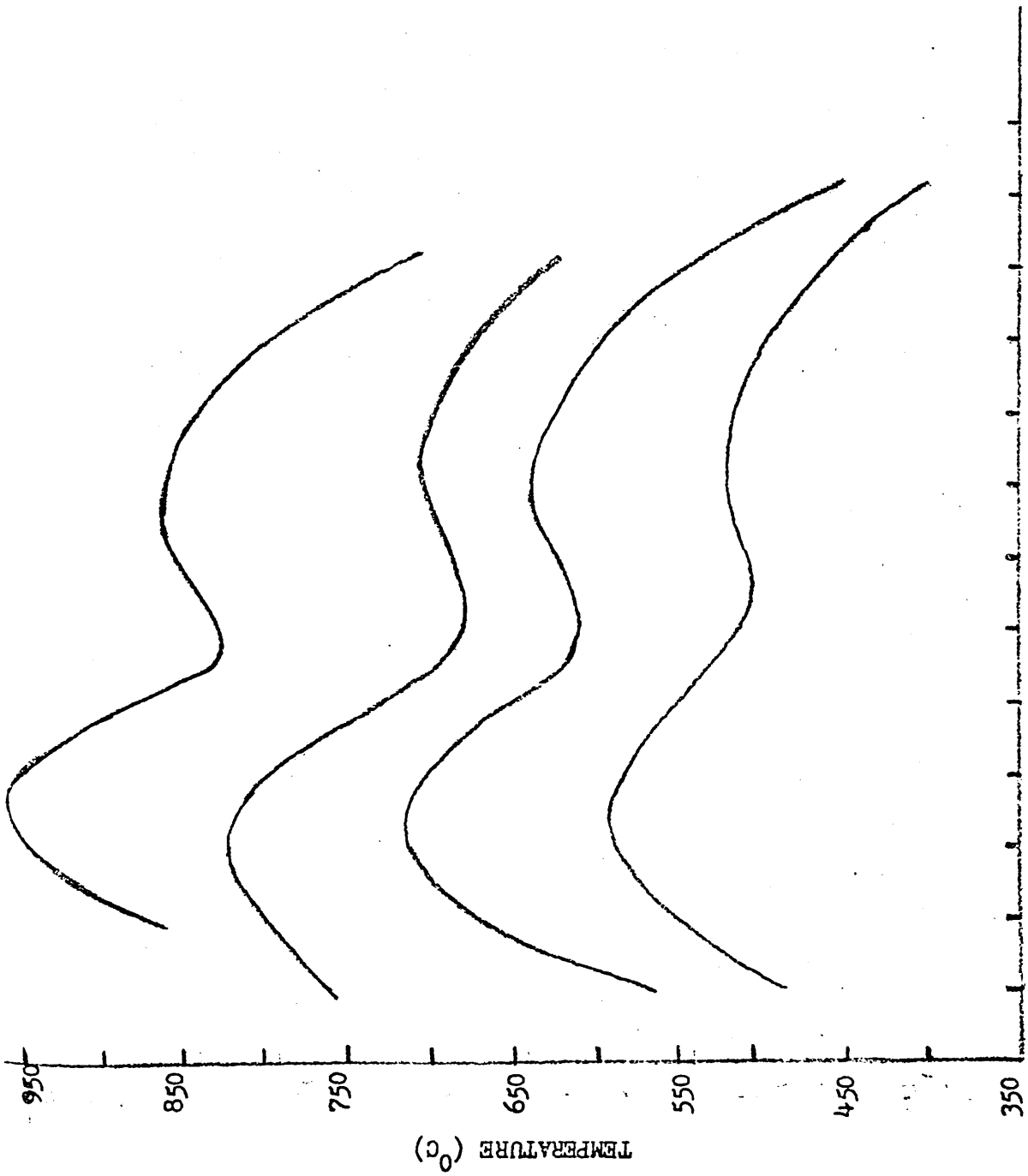

Appendix A-1 Temperature profile in working region

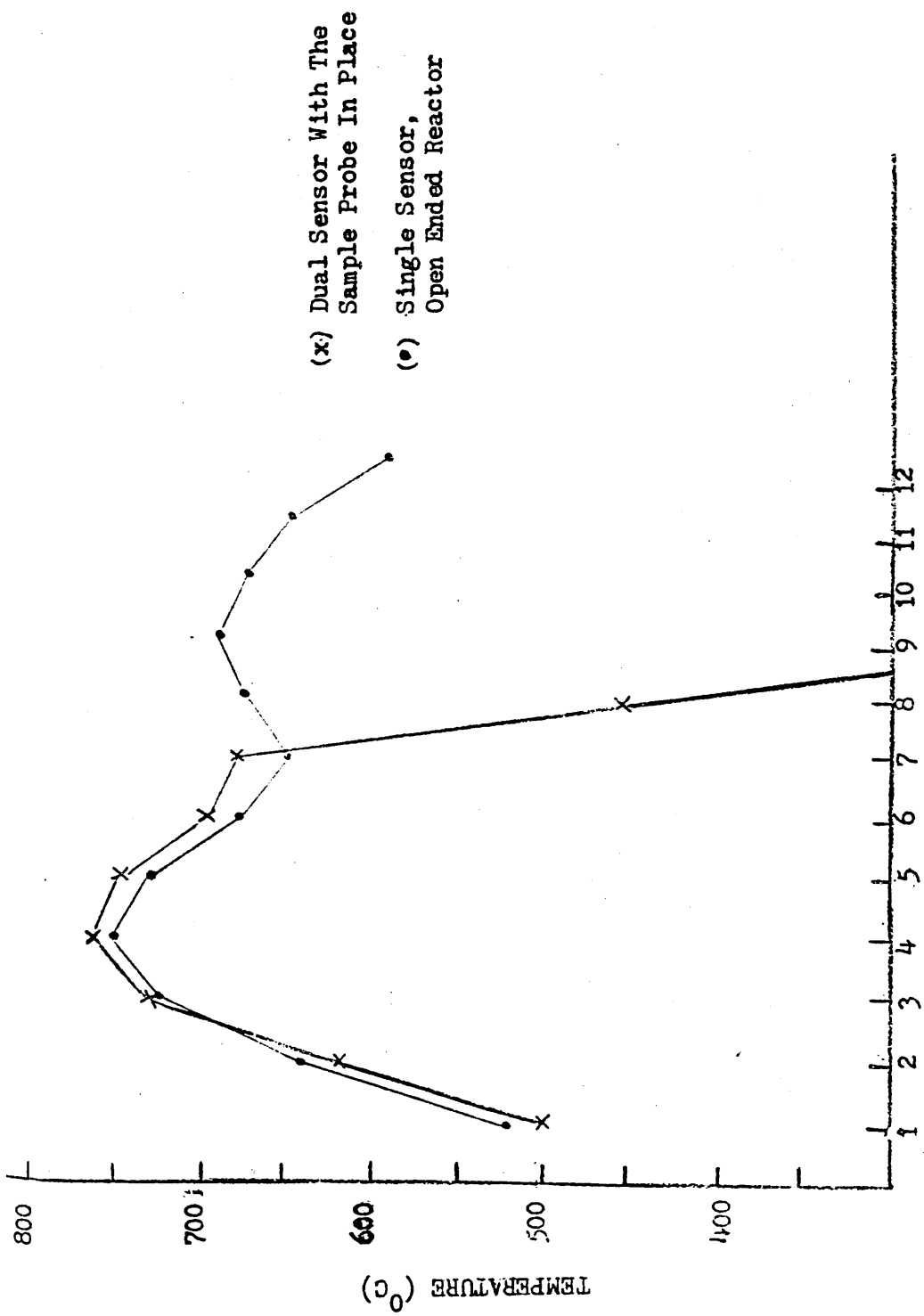

Appendix A-2 Temperature profile in working region

Appendix A-3

Helium Flow Rate Setting for the Laminar Flow Reactor

Peak temperature ^{o}C	SCCM Helium
600	6248.5
700	5606.5
800	5084
900	4651
1000	4285.6
1100	3973.5

Appendix A-4

Relationship between Mesh # and Particle Size

U.S. Standard Mesh #	Particle Size
80	177
100	149
120	125
140	105
170	88
200	74
230	63
270	53
325	44

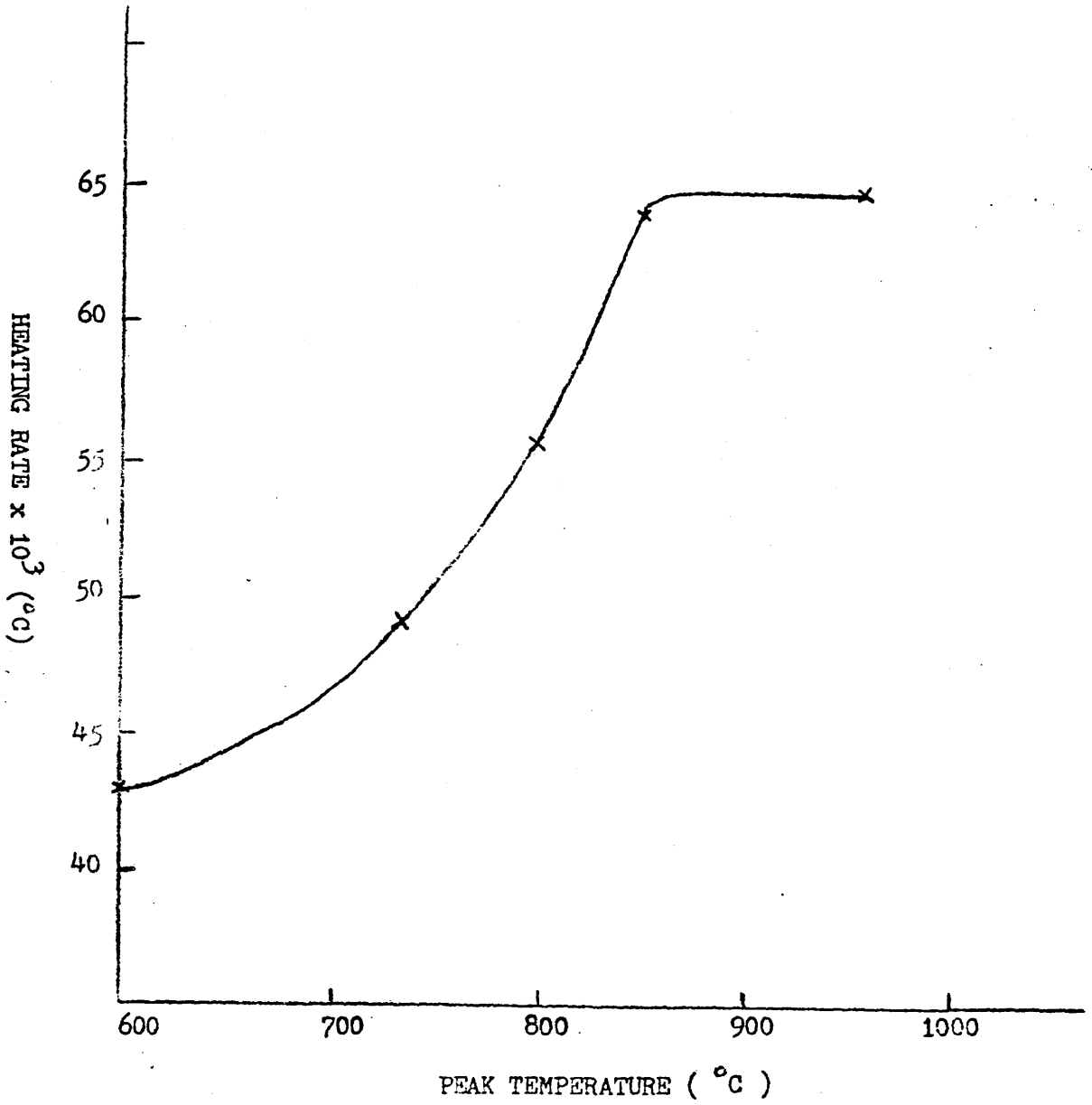

Appendix A-5 Heating rate of the laminar flow reactor

Appendix A-6

Determination of Final Particle Settling Velocity
v_f = final settling velocity (ft/sec)

Average temperature (°C)	270 μm v_f	200 μm v_f	180 μm v_f
600	4.08	2.42	1.96
700	3.80	2.30	1.83
800	3.48	2.10	1.68
900	3.37	2.03	1.62

Appendix A-7

Calibration of TZG 3

Counter number	Standard 4X (μm)	Standard 10X	Reduced 4X (μm)	Reduced 10X	Counter number	Standard 4X (μm)	Standard 10X	Reduced 4X (μm)	Reduced 10X
1	26.8	10.9	9.5	3.8	25	320.5	130.6	108.3	43.5
2	39.0	15.9	13.5	5.4	26	332.7	135.6	112.4	45.1
3	51.4	20.9	17.6	7.1	27	344.9	140.5	116.6	46.8
4	63.6	25.9	21.6	8.7	28	357.3	145.6	120.7	48.4
5	75.8	30.8	25.6	10.3	29	369.5	150.4	124.9	50.2
6	88.0	35.8	29.7	12.0	30	381.7	155.4	129.0	51.8
7	100.2	40.7	34.0	13.6	31	393.9	160.3	133.0	53.4
8	112.6	45.8	38.0	15.2	32	406.1	165.3	137.3	55.1
9	124.8	50.8	42.3	17.0	33	418.5	170.3	141.4	56.7
10	137.0	55.7	46.3	18.6	34	430.7	175.3	145.6	58.5
11	149.2	60.7	50.3	20.2	35	442.9	180.3	150.0	60.1
12	161.4	65.6	54.6	21.9	36	455.1	185.2	153.7	61.7
13	173.8	70.7	58.7	23.5	37	467.3	190.2	158.0	63.4
14	186.0	75.6	62.9	25.3	38	479.7	195.2	162.0	65.0
15	198.2	80.6	67.0	26.9	39	491.9	200.2	166.3	66.8
16	210.4	85.5	71.0	28.5	40	504.1	205.2	170.3	68.4
17	222.6	90.5	75.3	30.2	41	516.3	210.1	174.4	70.0
18	235.0	95.7	79.3	31.8	42	528.5	215.1	178.7	71.7
19	247.2	100.7	83.6	33.6	43	540.9	220.1	182.7	73.3
20	259.4	105.7	87.6	35.2	44	553.1	225.1	187.0	75.1
21	271.5	110.6	91.7	36.8	45	565.3	230.1	190.0	76.7
22	283.8	115.6	96.0	38.5	46	577.5	235.1	195.1	78.3
23	296.2	120.7	100.0	40.1	47	589.6	240.0	199.3	80.0
24	308.3	125.6	104.3	41.9	48	602.1	245.0	203.4	81.6

Appendix A-8

Nomenclature of Table 3-1

a_0	Initial bubble size.
a_i, a_j	Radius of bubble i,j.
$\dot{a}_i$	Growth rate of bubble i
b_i, b_j	Distance between the particle wall and the center of bubbles i,j.
d_{min}	Distance to the nearest surface through which volatile can escape.
E_d	Activation energy of the secondary reaction.
F	Volatile flux per unit surface area.
k_d^o	Preexponential factor of the secondary reaction rate constant.
k_d	Secondary reaction rate constant.
M_0	Original coal mass.
M_p	Coal mass.
p_∞	Pressure of surroundings.
q_d	Rate of secondary reaction per unit area.
Q_d	Rate of the secondary reaction per bubble.
R	Radius of particle or universal gas constant.
W	Total mass loss of particle.
w	Mean molecular weight of the bubble.
x_i, x_j, x_k y_i, y_j, y_k z_i, z_j, z_k	Spatial coordinates of bubble i,j,k.
Λ_b	Bubble generation probability distribution function.

λ_{a0}	Initial bubble size probability distribution function.
μ	Viscosity.
σ	Surface tension of bubble shell.
ρ_p	Density of particle phase.
v_i, v_j, v_k	Mass of bubble i,j,k.
$\dot{v}_i$	Rate of mass accumulation inside bubble i.
$\frac{dx}{dt}$	Rate of volatile generation per unit mass of original coal.

BIBLIOGRAPHY

1. Andrade, E.N. DA C., "The Viscosity of Liquids", Nature, London, 125, 362 (1930).
2. Anthony,D.B., "Rapid Devolatilization and Hydrogasification of Pulverized Coal," Sc.D. Thesis, Dept. of Chemical Engineering, Mass. Inst. Tech., Cambridge (1974).
3. Anthony, D.B., J.B. Howard, H.C. Hottel, and H.P. Meissner, "Rapid Devolatilization of Pulverized Coal," Fifteenth Symposium (International) on Combustion, p.1303, The Combustion Institute, Pittsburgh, Pa. (1975).
4. Anthony, D.B., and J.B. Howard, "Coal Devolatilization and Hydrogasification," AIChE J., 22, No.4, 625 (1976).
5. Attar, A., "Bubble Nucleation in Viscous Material Due to Gas Formation by a Chemical Reaction-Application to Coal Pyrolysis," Prepublished Paper, University of Texas, (1977).
6. Audibert, E., "Transient Fusion of Coal," Fuel, 5, 6, (1927).
7. Bond, R.L., and D.H.T. Spencer, Industrial Carbon and Graphite, p.231 Soc. Chem. Ind., London, England, (1958).
8. Brown, H.P., and P.L. Waters, "The Function of Solvent Extraction Products in the Coking Process II - A Theory of the Mechanism of Thermal Softening," Fuel, 45, 41 (1966).
9. Chermin, H.A.G., and Van Krevelen, D.W.,"Chemical Structure and Properties of Coal XVII - A Mathematical Model of Coal Pyrolysis," Fuel, 36,85 (1957).

10. Ergun, G., H.J. O'Donnell, and B.C. Parks, "Microscopic Studies of the Rate of Thermal Decomposition of Petrographic Components of Coal," Fuel, 38 , 205 (1959).

11. Evans, D.G., and J.A. Herman, "The Porosity of Brown Coal Char," Fuel, 49 , 110 (1970).

12. Feldmann, H.F., Kiang, K.D., and Yavorsky, P.M.,"Fluidization Properties of Coal Char," Am. Chem. Soc., Div. of Fuel Chem., Preprints 15 , 3 , 62-76 (Sept,1971).

13. Franklin, R.E., "A Study of the Fine Structure of Carbonaceous Solids by Measurements of True and Apparent Densities Part I - Coals," T. Faraday Soc., 45 , 274 (1949a)

14. Gibson, J., and G.H. Gregory Carbonization of Coal, pp. 11-12, London, Mills and Boon, (1971).

15. Hirsch, P.B., Proc. Ray. Soc., A226 143 (1954).

16. Lau, E. Personal Communication.(May, 1977).

17. Lewellen, P.C., "Product Decomposition Effects in Coal Pyrolysis", M.S. Thesis, Chemical Engineering Dept., M.I.T. , Sept. (1975).

18. Lightman, P. and P.J. Street, "Microscopical Examination of Heat Treated Pulverized Coal Particles," Fuel, 47 , 7 , (1968).

19. Mason, D.M., and F.C. Schora Jr., "Coal and Char Transformation in Hydrogasification," in Fuel Gasification, p.18, Advances in Chemistry Series, No. 69, Am. Chem. Soc., Washington D.C. (1967).

20. Neavel, R.C., "Coal Plasticity Mechanism: Inferences From Liquefaction Studies," Symposium on Plasticity and Agglomeration of Coal, U.S.

Energy Research and Development Administration, Morgantown, W.Va., (May 5-6,1975).

21. Newall, H.E., and F.S. Sinnatt,"The Carbonization of Coal in the Form of Fine Particles I - The Production of Cenospheres," Fuel, 3 , 4 , 24 (1924).

22. Newall, H.E., and F.S. Sinnatt, "The Study of Cenospheres, II," Fuel, 5 , 3 , 35(1926).

23. Newall, H.E., and F.S. Sinnatt, "The Study of Cenospheres IV", Fuel, 6 , 398 , (1927).

24. Sinnatt, F.S., "The Formation and Structure of Cenospheres," J.Soc. Chem. Ind., 47 , 152 T(1928).

25. Sinnatt, F.S., "Some Properties of Coal Dust and Pulverized Coal," Fuel, 8 , 362 (1929).

26. Sinnatt, F.S., A. McCulloch, and H.E. Newall, " The Carbonisation of Particles of Coal," Fuel, 6 , 398 (1927).

27. Spackman, W., and Berry, W., "Thermal Behavior of Coal Constituents", motion picture produced at the Pennsylvania State University, (September 1968).

28. Street, P.J., R.P. Weight, and P. Lightman, "Further Investigations of Structural Changes Occuring in Pulverized Coal Particles During Rapid Heating," Fuel, 48 , 343 (1969).

29. Suuberg, E., Personal Communication (May,1977).

30. Van Krevelen, D.W., Coal , Elserin Publishing Co., Amsterdam, (1961).

31. Van Krevelen, D.W., F.J. Huntjens, and H.N.M. Dormans, "Chemical Structure and Properties of Coal XVI - Plastic Behavior on Heating,"

Fuel, 35,462 (1956).

32. Waters, P.L., "Rheological Properties of Coal During the Early Stages of Thermal Softening," Fuel, 41 , 3 (1962).

33. Woods, M.F., G.M. Habberjam, K.Elsworth, and S. Bennett,"The Effect of Maceral Composition on the Binderless Briquetting of Hot Char," Fuel, 46 , 193 (1967).

34. Franklin, R.E., "A Study of the Fine Structuresof Carbonaceous Solids by Measurements of True and Apparent Densities Part II- Carbonized Coals," Fuel, 45 , 668 (1949b).